Submitted to: Proceedings of the Health Physics Society 2008 Professional Development School - Topics in Accelerator Health Physics (Oakland CA, January 2008)

Induced Radioactivity at Accelerators

J. Donald Cossairt

Introduction

In this chapter the production of induced radioactivity at accelerators is described. The discussion begins with a review of the basic principles of the production of radioactivity. It proceeds with a discussion of the activation of accelerator components including some generalizations that may be used for practical health physics applications. Production and propagation of accelerator-produced radioactivity in environmental media such as air, soil, rock, and water also is addressed and introductory material connecting meteorology and hydrogeology with the transport of this radioactivity is included. The use of induced radioactivity in radiation measurements at accelerators concludes this chapter. To maintain harmony with nearly universally accepted practice, cgs units (i.e., centimeters, grams, and seconds) are, at some points, employed.

General Principles

The Cross Section Concept

The concept of the cross section is an extremely important physical concept in describing particle interactions and is of particular importance to the topic of this chapter. The cross section represents the effective "size" of the atom or nucleus for some particular interaction. Consider a beam of particles of fluence Φ (particles cm^{-2}) incident on a thin slab of absorber of thickness dx. The absorbing medium has N atoms cm^{-3}. $N=\rho N_A/A$, where ρ is the material density (g cm^{-3}), N_A is Avogadro's number (6.02214 x 10^{23} g-molel^{-1}), and A is the atomic mass number. The decrease in fluence $d\Phi$ due to the loss of incident particles that interact in a small thickness of

material dx is given by

$$-d\Phi = \sigma N \Phi dx, (1)$$

where the cross section σ of the given process has units of area, typically in cm^2. Cross sections are often tabulated in units of barns (1.0 barn=10^{-24} cm^2). Submultiples such as the mb (10^{-3} barn, 10^{-27} cm^2) are often used. If only one physical process is present with no others operative and if one starts with an initial fluence Φ_0, this integrates after some finite material thickness x to

$$\Phi(x) = \Phi_o e^{-N\sigma x} . (2)$$

Pertaining to radioactivation, σ refers to the cross section for producing a particular radionuclide.

The Activation Equation

In principle, induced radioactivity can be made at all accelerators capable of producing particles above some reaction threshold pertinent to the activation process of interest. When the accelerated beam particle strikes a nucleus, the resultant nuclear reactions can create a different nuclide that may or may not be radioactive. The activity of a given radionuclide refers to the number of atoms that decay per unit time. The customary unit of activity is the Curie (Ci). One Curie, historically defined to be the activity of one gram of natural radium, is 3.7 x 10^{10} decays per second. The SI unit of activity is the Becquerel (Bq), defined as 1.0 decay per second, with submultiples such as the Gbq commonly used. A related quantity of importance is the specific activity, defined as the activity per unit volume (e.g., pCi cm^{-3}, Bq cm^{-3}) or alternatively as the activity per unit mass (e.g., pCi g^{-1}, Bq g^{-1}), an ambiguity beyond the control of this author!

Radioactive decay is a random process characterized by a mean-life (units of time), denoted by τ, and its reciprocal (units of inverse time), the decay constant λ. Care needs to be taken with the use of this particular symbol since it also commonly denotes mean free path. If a total of $N_{tot}(t)$ atoms of a radionuclide are present at time t, the total activity $A_{tot}(t)$ is determined

by the random nature of radioactive decay to be

$$A_{tot}(t) = -\frac{dN_{tot}(t)}{dt} = \frac{1}{\tau} N_{tot}(t) = \lambda N_{tot}(t) \quad .(3)$$

If at time t=0, $N_{tot}(0)$ atoms are present, then this simple differential equation has the following solution at some later time t=T;

$$A_{tot}(T) = \lambda N_{tot}(0) \exp(-\lambda T) = A_{tot}(0) \exp(-\lambda T) \quad .(4)$$

Likely for historic reasons, the time required for decay to half of the original activity, the half-life $t_{1/2}$, is commonly tabulated. $t_{1/2}$, is related to the mean-life τ by the following:

$$\tau = \frac{1}{\ln 2} t_{1/2} = \frac{1}{0.693} t_{1/2} = 1.442 t_{1/2} \quad .(5)$$

In this chapter values of half-lives are taken from the authoritative compilation of the National Nuclear Data Center (Tuli 2005).

The most simple activation situation at accelerators is that of the steady irradiation of some material by a spatially uniform flux density of particles that begins at time t=0 and continues at a constant rate for an irradiation period ending at t=t_i. This is followed by a decay period commonly called the cooling time denoted t_c, a period of time that begins at t=t_i and ends at t=t+t_c. For this simple situation, self-absorption of the incident particles by the target is ignored, as is the fact that a whole spectrum of particles of multiple types could be incident. Within these simplifications the process of producing the radioactivity is characterized by a single average cross section σ. In the generalized situation the value of this cross section must be obtained from averaging over the energy spectra of the particles incident.

The number of atoms of the radionuclide of interest per unit volume will thus be governed by the following equation during the period of the irradiation:

$$\frac{dn(t)}{dt} = -\lambda n(t) + N\sigma\phi \text{ ,(6)}$$

where $n(t)$ is the number density (cm^{-3}) of atoms of the radionuclide of interest at time t. As before, N is the number density of "target" atoms (cm^{-3}), σ is the production cross section (cm^2) and ϕ is the flux density ($cm^{-2}\ s^{-1}$) of incident particles. On the right hand side of the above equation, the first term represents the rate of loss of the radionuclide through decay during the irradiation while the second term represents the rate of gain of the radionuclide through the production reaction under consideration. The equation has the following solution for $0<t<t_i$:

$$n(t) = \frac{N\sigma\phi}{\lambda}\left(1 - e^{-\lambda t}\right). \text{ (7)}$$

Using Eq. (3) the specific activity $a(t)$ induced in the material as a function of time during the irradiation is $a(t)=\lambda\, n(t)$. For $0<t<t_i$ the value of specific activity in Bq arises naturally for t in seconds;

$$a(t) = N\sigma\phi\left(1 - e^{-\lambda t}\right) \text{ (Bq cm}^{-3}\text{).(8)}$$

Specific activity in units of Curies $cm^{-3}$is obtained by simply dividing the result by the conversion factor of 3.7×10^{10} Bq Ci^{-1}. At the end of the irradiation ($t=t_i$), the specific activity is

$$a(t_i) = N\sigma\phi\left\{1 - \exp(-\lambda t_i)\right\} \text{ (Bq cm}^{-3}\text{),(9)}$$

so that the specific activity as a function of time is characterized by a buildup from zero to the saturation concentration value proportional to $N\sigma\phi$ for infinitely long irradiations. The constant of proportionality is conveniently unity for time in seconds and activity in Bq. After the irradiation has ceased ($t>t_i$), the specific activity as a function of the cooling time $t_c=t-t_i$ will obviously decay exponentially. The result of this process is described by the activation equation;

$$a(t_c) = N\sigma\phi\left\{1 - \exp(-\lambda t_i)\right\}\left\{\exp(-\lambda t_c)\right\} \text{ (Bq/cm}^3\text{).(10)}$$

To obtain total activities in some object in situations where uniform flux densities of particles of constant energy are incident on a homogeneous target, one can simply multiply by the volume of the target material. Or, in more complex cases involving non-uniform flux densities, one can integrate the above over the sub-volumes of the target. Where a spectrum of energies is inolved, more complex integrations need to be performed.

Activation of Components at Electron Accelerators

General Phenomena

At electron accelerators the direct interactions of electrons in material results in the copious production of photons. Through various nuclear reaction channels, these photons then proceed to produce charged particles and neutrons that then interact further with material to produce radioactivity. In general, if the facility is properly shielded against prompt radiation, the radioactivity hazard will be confined to accelerator components and the interior of the accelerator enclosure. The experience at most accelerators, not limited to the situation at electron accelerators, is that the vast majority of the dose equivalent received by the workers is due to maintenance activities on radioactivated components, handling and moving of activated items, radiation surveys, and radioactive waste handling activities rather than exposure to the prompt radiation fields. An understanding of the production of radionuclides can help reduce personnel exposures through the selection of more appropriate machine component materials and the optimization of decay ("cool-down") times recommended after the beam has been turned off.

At electron accelerators a major, often dominant, contributor to radioactivation is due to photons radiated as a result of the bremsstrahlung process experienced by the electrons interacting with matter. This is due to the fact that the nuclear reaction cross sections of electrons are about two orders of magnitude smaller than those of photons (Swanson 1979a). These

photons then produce the radioactivity through photonuclear reactions. Some familiarity with the relevant cross sections of these reactions is useful. “Global” results spanning the periodic table have been compiled by Barbier (1969). Representative examples are given in Fig. 1. In general, the fewer the number of nucleons that are removed in such reactions, the larger the cross section will be. Correspondingly, the cross sections will be much smaller for rare processes such as the photo-pion reactions shown also in Fig. 1.

Results for Electrons at Low Energies

It is now appropriate to provide more details. Swanson (1979a) utilized the methodology of "Approximation B" of the classic analytical electromagnetic shower theory (Rossi and Griesen 1941) to estimate saturation activities rates in various materials representative of the outcomes of the showers. This work represents an important extension of the shower theory to the practical consequence of radioactivation, an application likely not foreseen by Rossi and Griesen. Since the energy domain below about 35 MeV is characterized by rapidly varying cross sections, Swanson provided energy-dependent results. Here only reactions of the type (γ,n), (γ,p), (γ,np), and (γ,2n) were considered. Other reactions were ignored due to higher energy thresholds and small cross sections. Swanson points out that the dependence of the induced activity as a function of energy will generally follow that of the neutron yields given here in Fig. 2 (Swanson 1979b). In Swanson's calculations, the material in question absorbed all of the beam power and had been irradiated for an infinite time with no cooldown [$t_i=\infty$, $t_c=0$ in Eq. (10)]. Thus, so-called saturation activities are calculated and normalized to the incident electron beam power.

Selected results of these calculations, taking into account the natural isotopic abundances and individual reaction thresholds, are provided in Table 1. The results are likely accurate to about $\pm$ 30 per cent. At these low energies the distribution of the radioactivity can often

approximately be taken to be that of a point source for calculating the residual absorbed dose rates. Table 1 provides the specific gamma-ray constant Γ for each tabulated radionuclide. This parameter connects induced activity with the absorbed dose rate at a distance of one meter for point source conditions accounting for all the photons emitted by the decaying radionuclide, including those emitted secondarily by internal bremsstrahlung as well as annihilation radiation due to β^+ emission manifested in the form of a pair of 0.511 MeV photons. For point sources, exposure rates at other distances can be calculated by incorporating the inverse square law. Due to general usage, results using both SI and "customary" units of measure are provided. In Table 1, and elsewhere in this chapter, nuclear isomeric states (i.e., isomers) are identified by the letter "m" follwing the mass number affixed to the chemical symbol (e.g., ^{26m}Al). Isomers are nuclear excited states with exceptionally long lifetimes; sufficiently lengthy to be of importance to the topic of accelerator-produced radioactivity. Most isomers decay by γ-ray emission to the ground state of the same isotope, but other decay modes exist for some such states.

Results for Electrons at Higher Energies

For higher energy electrons, more reaction channels become available but the energy dependence is diminished. Swanson (1979a) has also provided useful results in this energy domain and examples are provided in Table. 2. The results are valid to about a factor of two for any beam energy E_o that is well above the nuclide production threshold. Specific gamma-ray constants for point source conditions Γ, reaction energy thresholds, saturation activities, and absorbed dose rates are provided. Also given and denoted by the somewhat esoteric symbol $\Sigma f\sigma$ are the integral radionuclide production cross sections (summed over parent isotopes present in the tabulated material) per MeV of electron beam energy. The quantity $\Sigma f\sigma$ is a useful one because of the dominance, and lack of energy dependence, of the photoneutron production

process of electrons interacting in matter. The electrons are assumed to be totally absorbed in the material with no self-shielding effects. As a simplification, the distribution of radioactivity within the material is assumed to be uniform. The results are, again, presented for saturation conditions ($t_i = \infty$, $t_c = 0$) for the compositions of materials described in the table.

Cooling curves have been developed by Barbier (1969) for high energy electrons incident on various materials for an infinite irradiation at the rate of one electron per second. The results are given in Fig. 3, again per MeV of incident electron energy, for an infinite irradiation time t_i. In this figure results are given for the absorbed dose rates (Gy h^{-1}) per electron s^{-1} assuming the applicability of point source conditions. The lack of strong energy dependence (i.e., the result that allows one to scale photon and neutron production rates with incident beam power) and the simplicity of the photoneutron spectra make possible these rather uncomplicated results.

Activation of Components at Proton and Ion Accelerators

General Phenomena

Protons having energies above a few MeV kinetic energy will produce radioactivity upon interacting with matter. This will also occur for other ions above a comparable specific energy of about 10 MeV/nucleon. In some special cases radioactivity can be produced at much lower energies due to exothermic nuclear reactions that either produce radionuclides directly or emit neutrons capable of inducing radioactivity through their secondary interactions. As with electron accelerators, if a given accelerator is properly shielded against prompt radiation and has proper access controls to avoid direct beam-on exposure, the induced radioactivity is very likely to be the dominant source of occupational radiation exposure.

For the lower incident energies (i.e., below about 30 MeV), one is first concerned with production of radionuclides by such processes as (p,γ) as well as single- and multi-nucleon

transfer reactions. While the details of the total cross sections for such reactions are complex, the systematics and approximate energy dependencies are globally well-understood. The concept of the Q-value Q_v is useful. Q_v is the energy released by the reaction and is defined in terms of the rest masses m_i of the particles participating in the nuclear reaction $m_1+m_2->m_3+m_4$ as

$$Q_v = [(m_1 + m_2) - (m_3 + m_4)]c^2 \quad (11)$$

The shorthand notation of $m_2(m_1,m_3)m_4$ is commonly used for such reactions where usually, but not exclusively, the projectilve is represented by m_1 while the less massive emitted particle is denoted m_3. $Q_v>0$ implies an exothermic reaction while endothermic reactions ($Q_v\leq 0$) are characterized by a threshold energy E_{th} related to the absolute value of Q_v;

$$E_{th} = \frac{m_1 + m_2}{m_2}\left|Q_v\right| \quad (12)$$

Barbier (1969) has addressed activation by many types of particles in a global manner. Samples of some of these results are provided concerning specific reaction processes at a variety of energies in Figs. 4 and 5. The plotted results are for inclusive reactions, so-called because they include all reaction channels that can lead to the indicated radionuclide. At the higher energies, they, for example, could include spallation processes and pion ($\pi^{\pm}$)or kaon ($K^{\pm}$) production in addition to multi-nucleon transfers prolific at lower energies. Some results for the light elements are especially important for environmental radiation calculations while those for iron and copper targets are of great importance due to the universal presence of those elements at accelerators.

Thick target yields of radionuclides for targets spanning the periodic table have been systematically studied by Cohen (1978) for a number of nuclear processes spanning the periodic table. A thick target in this context is one in which the particles of interest are ranged out by ionization. Fig. 6 is a representative plot of the general features of excitation functions of such

nuclear reactions. Specific processes may vary considerably from this behavior since "resonances" at specific nuclear excited states have been ignored. Table 3 lists a variety of such nuclear reactions along with the range of values of energy above threshold at which the radioactivity production rate has risen to 0.1% of the saturation value and also the range of saturation values for the production of radioactivity. These results span the periodic table. It is assumed that the target thickness comfortably exceeds the range of the incident ion and that the irradiation period greatly exceeds the half-life of the radionuclide of interest. For shorter bombarding periods one corrects by multiplying by the factor [1-exp(-λt_i)]. Over the energy domain of these curves, the importance of activation by secondary particles is small compared to that encountered at higher energies. For detailed work, the scientific literature should be searched for detailed results.

Methods of Systematizing Activation Due to High Energy Hadrons

For proton and ion accelerators of higher energy, the neglect of secondary reactions and the restriction to few and multi-nucleon transfer reactions can be a serious deficiency in the accuracy of estimation of induced radioactivity because of the rise in importance of such processes as spallation. Below a kinetic energy of about 40 MeV or so only few-nucleon transfer reactions are available. The variety of radionuclides that can be produced increases as one increases the bombarding energy because more thresholds are exceeded. As a general rule, at high energies ($E_O \approx 1$ GeV or above), one must consider that all radionuclides in the periodic table that have mass numbers less than that of the material exposed to the flux of hadrons may be produced. Of course, many of these are of little significance due to short lifetimes and small production cross sections.

Table 4 lists radionuclides typically encountered in high energy proton and ion

accelerators along with their half-lives. Here only nuclides with half-lives between 10 minutes and 5 years are listed. In Table 4 "pure" β^- (electron) emitters (those that emit no γ-rays in their decays) are not included. Pure β^- emitters generally present minimal exposure hazards in routine maintenance activities at accelerators, as compared with γ-ray emitters, since all the radionuclides are produced as "volume activation" throughout the materials comprising accelerator components. The resultant self-shielding of most of the decay electrons compared with the less effective shielding of the more penetrating γ-rays reduces the relative importance of the former compared with the latter in terms of the personnel dose equivalent. In contrast, "pure" β^+ (positron) emitters are listed in Table 4 due to the generation of the pairs of 0.511 MeV photons that result from annihilation of the positrons with electrons in matter. Approximate thresholds and high energy cross sections for production of these radionuclides by protons, generally taken from Barbier (1969), are also provided where available.

Sullivan-Overton Approximation. A systematic way of addressing the great multiplicity of radionuclides produced in accelerator components by high energy particles is highly desirable since it is often not practical to handle them all separately. Global properties of the distribution of radionuclides are found to be useful. Sullivan and Overton (1965) have treated this problem in an elegant manner reprised here. The initial starting point is a modification of Eq. (10) describing the dose rate as a function of irradiation and cooling times t_i and t_c;

$$\delta(t_i, t_c) = G\phi\left[1 - \exp(-\lambda t_i)\right]\exp(-\lambda t_c), \quad (13)$$

where $\delta(t_i, t_c)$ is the absorbed dose rate and ϕ is the flux density of the incident particles. G is a function dependent on the energy of the beam, the types of secondary particles produced, the isotopic composition of the irradiated component, the geometry, the energy of the γ-rays

produced, and the attenuation coefficients for the γ-rays produced.

If the number of radionuclides produced by the irradiation having decay constants in the interval between λ and $\lambda+d\lambda$ is represented by the differential dm then the corresponding increment in absorbed dose rate due to them $d\delta(t_i, t_c)$ is given by

$$d\delta(t_i, t_c) = dmG\phi\left[1-\exp(-\lambda t_i)\right]\exp(-\lambda t_c)\,. (14)$$

A result from the body of data is that on average one can assume that the radionuclide production cross sections under consideration are independent of both half-lives and particle energies. Further, if it is assumed that the value of G is independent of λ, or its dependence on λ is small compared to other factors, then one can integrate

$$\delta(t_i, t_c) = G\phi\int_{\lambda_o}^{\infty} d\lambda \frac{dm}{d\lambda}\left[1-\exp(-\lambda t_i)\right]\exp(-\lambda t_c)\,. (15)$$

Here λ_o is the shortest decay constant, corresponding to the longest mean-life, to be considered. Fig. 7 is a plot of the number of radionuclides as a function of half-life $t_{1/2}$ that have half-lives less than that particular half-life for several choices of atomic mass number A. This corresponds to the distribution of radionuclides that could be produced in a target of mass number A irradiated by intermediate or high energy hadrons or heavy ions. As one can see, these cumulative distributions are well-described for half-lives between about 10^{-3} and 10^{3} days by

$$N(t_{1/2}) = a + b\ln(t_{1/2})\,, (16)$$

where $N(t_{1/2})$ is the number of radionuclides with half-lives less than the value of $t_{1/2}$ and a and b are fitting parameters. Because of the one-to-one correspondence between values of $t_{1/2}$, τ, and λ, in this Sullivan-Overton approximation one can just as well write

$$m(\lambda) = a + b\ln\lambda\,, (17)$$

where $m(\lambda)$ is the number of radionuclides with decay constants *greater* than λ. Thus,

$$\frac{dm(\lambda)}{d\lambda} = \frac{b}{\lambda}. \quad (18)$$

Substituting into Eq. (15) one gets

$$\begin{aligned}\delta(t_i, t_c) &= Gb\phi \int_{\lambda_o}^{\infty} \frac{d\lambda}{\lambda}\left[1 - \exp(-\lambda t_i)\right]\exp(-\lambda t_c) \\ &= Gb\phi\left\{\int_{\lambda_o}^{\infty} \frac{d\lambda}{\lambda}\exp(-\lambda t_c) - \int_{\lambda_o}^{\infty} \frac{d\lambda}{\lambda}\exp\left[-\lambda\left(t_i + t_c\right)\right]\right\}\end{aligned}. \quad (19)$$

The changes of variables $\alpha = \lambda t_C$ [first term] and $\alpha' = \lambda(t_i + t_c)$ [second term] are helpful;

$$\delta(t_i, t_c) = Gb\phi\left\{\int_{\lambda_o t_c}^{\infty} d\alpha \frac{e^{-\alpha}}{\alpha} - \int_{\lambda_o (t_i + t_c)}^{\infty} d\alpha' \frac{e^{-\alpha'}}{\alpha'}\right\}. \quad (20)$$

Observing the identical integrands and rearranging the limits of integration;

$$\delta(t_i, t_c) = Gb\phi \int_{\lambda_o t_c}^{\lambda_o (t_i + t_c)} d\alpha \frac{e^{-\alpha}}{\alpha}. \quad (21)$$

The integration results in a series expansion found in standard tables of integrals;

$$\int_{x_1}^{x_2} \frac{e^{ax} dx}{x} = \left[\ln x + \frac{ax}{1!} + \frac{a^2 x^2}{2 \times 2!} + \frac{a^3 x^3}{3 \times 3!} + \ldots\right]_{x_1}^{x_2}. \quad (22)$$

Substituting,

$$\int_{\lambda_o t_c}^{\lambda_o (t_i + t_c)} \frac{e^{-\alpha} d\alpha}{\alpha} = \left[\ln \alpha - \alpha + \frac{\alpha^2}{4} - \frac{\alpha^3}{18} + \ldots\right]_{\lambda_o t_c}^{\lambda_o (t_i + t_c)}. \quad (23)$$

Evaluating, one obtains

$$\delta(t_i, t_c) = Gb\phi\left[\ln\left(\frac{t_i + t_c}{t_c}\right) - \lambda_o t_i + \ldots\right]. \quad (24)$$

Since λ_o approaches zero (corresponding to large mean-lives), the following is obtained:

$$\delta(t_i, t_c) \approx B\phi \ln\left(\frac{t_i + t_c}{t_c}\right), \quad (25)$$

where several constants are merged in the new parameter *B*.

***Gollon's Rules of Thumb*.** Gollon (1976) has further elaborated on these principles and collated four very useful "rules of thumb" for high energy hadron accelerators where the extranuclear hadronic cascade process produces the major fraction of the induced activity. These are extremely useful for approximate radioactivity estimates.

Rule 1:

For γ-ray emitters typical of those emitted by accelerator-produced radionuclides in the range of from about 100 keV to 10 MeV, many textbooks on health physics show that the absorbed dose rate *dD/dt* (Gy h^{-1}) at a distance *r* (m) from a "point" source is approximately given in terms of the source strength *S* (Gbq) and photon energies present $E_{\gamma i}$(MeV) by summing over all photons present, including their decay branching fractions as needed;

$$\frac{dD}{dt} = \left(1.08\times10^{-4}\right)\frac{S}{r^2}\sum_i E_{\gamma i} \quad .(26)$$

For *dD/dt* in rads h^{-1} at a distance *r* (m) from a source strength *S* (Ci), the coefficient 1.08 x 10^{-4} is replaced with 0.4. For non-point sources, a spatial integration must be performed.

Rule 2:

In many common materials, about 50 % of the nuclear interactions produce a radionuclide with a half-life longer than a few minutes. Further, about 50 % of these have a half-life longer than one day. Thus, approximately 25 % of the nuclear interactions produce a radionuclide having a half-life exceeding approximately one day. Individual inelastic nuclear interactions in materials are commonly called stars. This terminology is a legacy of early research using photographic emusion techniques to detect cosmic rays. The individual events in the developed emulsions had the appearance of “stars”, hence the name. One commonly speaks of total star density (e.g., stars cm^{-3}) or star density rate (e.g., stars cm^{-3} s^{-1}) or star density per

incident particle (e.g., stars cm^{-3} incident proton).

Rule 3:

This is Sullivan-Overton approximation [Eq. (25)]. In using this result, the geometry and material dependent factor *B* can often be determined empirically, or estimated by using Rule 2. Or, survey results at a known time following beam shutdown can be used to estimate the product $B\phi$. This result also appears to be valid also for intermediate energy heavy ion beams, for example at 86 MeV/nucleon (Tuyn et al. 1984).

Rule 4:

In a hadronic cascade, each proton or neutron produces about four inelastic interactions for each GeV of energy.

Some examples can illustrate the use of these rules of thumb. As one illustration, in a short target of 1/10 of an interaction length, approximately 10 % of an incident beam of 10^{11} protons s^{-1} will interact. Assume this has been occurring for several months (long enough to reach saturation production for many radionuclides) at this constant rate. Using Rule 2 in conjunction with the above rate, one determines that the decay rate after one day of the shutdown is $2.5x10^9$ Bq (68 mCi). If each of these decays produces a o1.0 MeV γ-ray, then Rule 1 will indicate an absorbed dose rate of 0.27 mGy h^{-1} (27 mrad h^{-1}) at a distance of one meter (point source conditions applicable).

Rule 3 is useful in predicting the absorbed dose rate at some future time after beam shutdown. Furthermore, this rule is not restricted to "point" sources but can be used for more massive ones, with suitable adjustments of the geometry factors. Using a measurement of absorbed dose rate early during a shutdown period to estimate $B\phi$ one can predict the "cooldown" at later times using Eq. (25) as a tool for planning radiological work. Rule 3 clearly

works for extended shields irradiated by secondary particles from a cascade.

Rule 4 can be used to crudely estimate the activation of a beam absorber by incident high energy particles when it is coupled with Rule 2 as illustrated by an example. A beam of 10^{12} 400 GeV protons s^{-1} (0.16 μA or 64 kW) produces a total of 4 x 400 x10^{12} stars s^{-1} in a beam absorber. If 25 % of these produce a radionuclide atom with a half-life greater than one day (Rule 2), then the total amount of the moderately long-lived radioactivity (at saturation) is

$$\frac{0.25 \text{ atoms}}{\text{star}} \times \frac{1.6\times10^{15}\text{stars}}{\text{sec}} = 4\times10^{14} \text{ Bq} = 4\times10^{5}\text{GBq} \quad .(27)$$

One could assume that a distance of 10 meters is sufficient to achieve "point source" conditions. If one further postulates that each decay is as a single 1.0 MeV photon, Rule 1 could be used to calculate an absorbed dose rate from such a source;

$$\frac{dD}{dt} = 1.08\times10^{-4}(1 \text{ MeV})\left(\frac{4\times10^{5}}{10^{2}}\right) = 0.43 \text{ Gy h}^{-1} .(28)$$

A valuable quantity used to quantify the absorbed dose rate *dD/dt* at the surface of a thick target is the danger parameter **D** developed by Barbier (1969) for a thick object irradiated by beam having a uniform flux density ϕ. If such a source of radioactivity subtends solid angle Ω at a point of concern, then

$$\frac{dD}{dt} = \frac{\Omega}{4\pi}\phi \, \mathbf{D} .(29)$$

For contact with a semi-infinite slab of uniformly irradiated material, the fractional solid angle factor ($\Omega/4\pi$) has the intuitively obvious value of 1/2. The danger parameter has the physical interpretation as the absorbed dose rate found inside a cavity of arbitrary form embedded in an infinite volume of a material that has been uniformly irradiated by a unit flux density (one particle s^{-1} cm^{-2}). Figs. 8 and 9 give representative examples of plots of **D** for several materials.

These curves can be used to predict cooling of various components around accelerators. Gollon (1976) has also provided "cooling curves" for iron struck by high energy protons. These are given in Fig. 10 and include both calculations by Armstrong and Alsmiller (1969) and empirical measurements at the Brookhaven National Laboratory Alternating Gradient Synchrotron (AGS), the now-decommissioned Fermilab Main Ring Accelerator, and a target station used for several years in the Fermilab Neutrino Experimental Area.

Of course situations arise where the determination of ϕ for use in the danger parameter equation is not at all simple. For example, one can have activation in a large object where the hadronic cascade is contributing numerous hadrons at a variety of energies from a multitude of directions. Fortunately, important features of activation phenomena have little or no correlation with energy. The chief of these is evidenced by the excitation functions of various reactions where the cross sections rise just above the threshold and then, somewhere in the region of tens of MeV above the threshold, level off. Furthermore, in general the cross sections for production of radionuclides by neutrons and protons (and even other ions and particles) do not differ greatly from each other (i.e., within one to two orders of magnitiude) at the higher energies.

The Utilization of Monte Carlo Star Densities in Activation Calculations

The "leveling-off" of the cross section as a function of energy has very important ramifications for activation. An important one is that for estimating activation, one can perform approximate calculations without performing integration over energy if one has some reasonable estimate of the hadron flux density above the reaction threshold of interest. An average effective cross section can then be used. Another feature of these excitation functions is the fact that the leveling off occurs in the region from a few 10's to a few 100's of MeV, precisely where relatively fast Monte Carlo hadron shielding calculations are available from several codes.

It is often possible to relate the flux density of high energy hadrons (i.e., those with energies above the leveling off) to the star density *S* calculated from such Monte Carlo calculations through the relationship

$$\phi(\boldsymbol{r}) = \frac{\lambda}{\rho}\frac{dS(\boldsymbol{r})}{dt}, \quad (30)$$

where $\phi(\boldsymbol{r})$, the flux density (cm^{-2} s^{-1}) at position vector at $\boldsymbol{r}$, is related to the rate of star density production *dS/dt* (stars cm^{-3} s^{-1}) at the same location. ρ (g cm^{-3}) is the density and λ (g cm^{-2}) is the interaction length. The value of $\phi(\boldsymbol{r})$ so determined could, in principle, be substituted into Eq. (29) for calculating absorbed dose rate due to residual activity using the Barbier danger parameter **D,** making suitable adjustments in the solid angle. However, the limitation of this approach is the fact that the Monte Carlo calculations may introduce a low energy (or low momentum) cutoff, typically around 50 MeV, perhaps not matched to the reaction threshold. In order to calculate dose equivalent rates, Gollon (1976) obtained the following formula:

$$\frac{dD(\boldsymbol{r})}{dt} = \frac{\Omega}{4\pi}\frac{dS(\boldsymbol{r})}{dt}\omega(t_i, t_c), \quad (31)$$

where the so-called omega factor (ω-factor) $\omega(t_i\ t_c)$ is related to the Barbier danger parameter. For iron, Gollon gives the following values for two useful situations:

$$\omega(\infty, 0) = 9 \times 10^{-2}\ (\mu\text{Gy h}^{-1})/(\text{stars cm}^{-3}\ \text{s}^{-1}), \quad (32a)$$

$$\omega(30\text{ d}, 1\text{ d}) = 2.5 \times 10^{-2}\ \mu\text{Gy h}^{-1})/(\text{stars cm}^{-3}\ \text{s}^{-1}). \quad (32b)$$

Estimates for additional ω-factors can be obtained by scaling results obtained by others (Armstrong and Alsmiller 1969; Gabriel and Santoro 1973) for selected values of t_i and t_c This has been done for three choices of values of t_i, and the results are shown in Fig. 11 for irradiated iron (Cossairt 1998). Curves of this type should be used with some degree of caution. They can readily be used to predict the relative "cooling" rates of various components around accelerators

with a fair degree of accuracy. Their use in the prediction of absolute dose equivalent rates due to activated accelerator components merits additional care. To do this, the geometric configuration should be simple and well-defined, the flux density of thermal neutrons should be a small component of the prompt radiation field, and the activation of other materials in proximity such as the enclosure walls should be taken into account. Cracks through the shielding materials can sometimes result in higher dose equivalent rates that are difficult to model and the transport of thermal neutrons in a shield can make a significant contribution to the dose equivalent rate.

Gollon (1976) also derived a simple relationship between dose rates involving cooling times different from "standard" ones for which values of **D** and ω are available. As stated previously, the dose rate after irradiation time t_i and cooldown time t_c is

$$\delta(t_i, t_c) = \sum_{\mu} A_{\mu} \left[1 - \exp(-\lambda_{\mu} t_i)\right] \exp(-\lambda_{\mu} t_c) \quad (33)$$

where the summation over index μ includes all relevant radionuclides with the product of flux density and geometry factors being absorbed in the quantity A_{μ}. Rearranging, Gollon obtained

$$\delta(t_i, t_c) = \sum_{\mu} A_{\mu} \left[\exp(-\lambda_{\mu} t_c) - \exp\left\{-\lambda_{\mu} (t_i + t_c)\right\}\right] = \delta(\infty, t_c) - \delta(\infty, t_i + t_c) \quad (34)$$

Thus, the infinite irradiation values can be used to determine any other combination of the times t_i and t_c. In fact, this formula may be used also with empirical results; for example radiation survey data, in order to predict future radiological conditions.

A reliable method to connect the production of "stars" in material (e.g., as calculated by a Monte Carlo code) with the production of atoms of some radionuclide is by the ratios of cross sections. Using vector notation to denote locations, at some point in space $\boldsymbol{r}$ the rate of production of atoms per cm^3 $n_i(\boldsymbol{r})$ of radionuclide i is approximately given by

$$\frac{dn_i(\boldsymbol{r})}{dt} \approx \frac{\sigma_i}{\sigma_{in}} \frac{dS(\boldsymbol{r})}{dt} = \frac{\Sigma_i}{\Sigma_{in}} \frac{dS(\boldsymbol{r})}{dt}, \quad (35)$$

where one essentially scales the star density production rate (e.g., stars cm^{-3} s^{-1}) by the ratio of the production (reaction) cross section for the nuclide of interest σ_i to the total inelastic cross section σ_{in} or, equivalently, by the ratio of the macroscopic cross sections Σ_i/Σ_{in}. The phenomena will obey the activation equation. The reason this is approximate is due to the standard concerns about constancy of cross sections with energy, the lack of perfect "matching" of effective reaction thresholds, etc.

Uniform Irradiation of the Walls of an Accelerator Enclosure

Special considerations apply to concrete shielding at accelerators. Ordinary concrete typically contains a partial density of about 0.04 g cm^{-3} of sodium. This "typical" value varies a great deal due to the variety of minerals that might be present in samples of concrete typical of different geographical locales. The significance of this seemingly small “accidental” additive is that all natural sodium is ^{23}Na. This nuclide has a relatively large cross section for the $^{23}Na(n,\gamma)^{24}Na$ thermal capture reaction; 535 mb at the most probable thermal neutron kinetic energy of 0.025 eV. Patterson (1958) determined an approximation for the average thermal neutron flux density ϕ_{th} in a concrete room;

$$\phi_{th} = \frac{1.25Q}{S} \ (cm^{-2}s^{-1}), \quad (36)$$

where Q is the number of fast neutrons produced per second in the enclosure and S is the inside surface area of the enclosure (cm^2). Thus, a substantial flux density of thermal neutrons can be present in an accelerator room and this flux can produce significant amount of ^{24}Na with its 14.95 hour half-life. The pair of relatively high energy photons emitted the decay of ^{24}Na [1.37

and 2.75 MeV, see Eq. (26)] further enhances the level of the residual radioactivity hazard.

Furthermore, while the dose due to activated components falls off radially with distance, if absorption by the air is not significant the photon flux density due to activation of the walls of an empty room uniformly irradiated by such thermal neutrons has been shown to be a constant. Thus, the absorbed dose rate due to the walls anywhere inside the enclosure will be equal to the absorbed dose rate at the wall. This has been shown to be true for cylinders (Armstrong and Barish 1969) and for the interior of mathematically "well-behaved" closed surfaces (Cossairt 1996). The general situation can readily be demonstrated by analogy to the Gauss Law in electrostatics (Konopinski 1981; Jackson 1999) as follows by examining the situation in Fig. 12.

Consider a simple, closed surface that emits an omnidirectional flux density of some particle ϕ_o (e.g., particles $cm^{-2}s^{-1}$) that is constant over the surface. One wants to calculate the flux density at some arbitrary point in space *P* within the surface. *P* is located at radius vector $\boldsymbol{r}$. Consider further the contributions of the particles emitted by some elemental area $d\boldsymbol{A}$ at *P* where $d\boldsymbol{A}$ is perpendicular to the surface at coordinate vector $\boldsymbol{r}$. The solid angle subtended at *P* by $d\boldsymbol{A}$ is

$$d\Omega = \frac{d\boldsymbol{A} \bullet \hat{\boldsymbol{n}}}{\left|\boldsymbol{r}' - \boldsymbol{r}\right|^2}, \quad (.37)$$

where the unit vector $\hat{\boldsymbol{n}}$ is given by

$$\hat{\boldsymbol{n}} = \frac{\boldsymbol{r}' - \boldsymbol{r}}{\left|\boldsymbol{r}' - \boldsymbol{r}\right|}. \quad (38)$$

But the increment of flux at point *P* due to elemental area $d\boldsymbol{A}$ is given by

$$d\phi = \frac{\phi_o}{4\pi} \frac{d\boldsymbol{A} \bullet \hat{\boldsymbol{n}}}{\left|\boldsymbol{r}' - \boldsymbol{r}\right|^2}. \quad (39)$$

Thus,

$$d\phi = \frac{\phi_o}{4\pi} d\Omega \text{ and } \int_{4\pi} \frac{\phi_o}{4\pi} d\Omega = \phi_o . \quad (40)$$

This phenomenon has been noticed at accelerators and results in "disappointment" in how little γ-ray exposure rates are reduced when activated accelerator components are removed from enclosures with walls that are, to some degree of approximation, “unformly” activated. Armstrong and Barish (1969) have calculated residual dose rates inside a cylindrical accelerator tunnel due to both the magnets and the concrete walls for 3 GeV protons incident on iron. They also included some other reactions due to higher energy neutrons, such as spallation, that are capable of also producing ^{24}Na from common ingredients of concrete. The results are shown in Fig. 13 for the surface at the tunnel wall. Thus, it can be important to minimize the amount of sodium in the concrete ingredients as an implementation keeping the doses as low as reasonably achievable (ALARA) to accelerator maintenance workers. When this phenomenon is operative, the “distance” part of the commonly used memory device of “time, distance, and shielding” for keeping doses as low as reasonably achievable (ALARA) is not available.

Activation and Environmental Media

Production of Airborne Radioactivity

Colleagues (Thomas and Stevenson 1988; Swanson and Thomas 1990) have presented a discussion, largely followed here, of the production of radioactivity in air. This results from the direct interactions of primary and secondary particles with the constituent target nuclei. Activated dust and gaseous emission from activated liquids are much less important. Table 5 gives the abundances and number densities of atoms of the most common stable isotopes found in the atmosphere both by volume percentage and in terms of the atomic density N_j. Patterson and Thomas (Pa73), have expanded the general activation equation to obtain the total specific

activity S (typically in units of Bq cm^{-3}) of an enclosed volume of radioactive air;

$$S = C\sum_i \left[\left\{ \sum_j N_j \bar{\sigma}_{ij\gamma}\phi_\gamma + \sum_j N_j \bar{\sigma}_{ijTH}\phi_{th} + \sum_j N_j \bar{\sigma}_{ijHE}\phi_{HE} \right\} \times \{1-\exp(-\lambda_i t_{irrad})\}\exp(-\lambda_i t_c) \right], \quad (41)$$

where ϕ_γ, ϕ_{TH}, and ϕ_{HE} represent the average photon, thermal neutron, and high energy particle flux densities. To avoid confusion, in this equation t_{irrad} is the irradiation time and and t_c is the cooling time. The $\bar{\sigma}_{ij_k}$ values are the corresponding cross sections averaged with the energy-dependent flux density over energy,

$$\bar{\sigma}_{ijk} = \frac{\int_{E_{\min}}^{E_{\max}} dE\sigma_{ijk}(E)\phi_k(E)}{\int_{E_{\min}}^{E_{\max}} dE\phi_k(E)}. \quad (42)$$

The limits of integration correspond to the three broad phenomenological ranges in the summation. The constant C in Eq. (41) converts the result to specific activity; equal to unity for activity in Bq cm^{-3} with units of length in centimeters and time in seconds. The outer sum over index i includes all radionuclides produced while the sum over the index j is over the different parent atoms found in air. The flux densities are, without further information, the average over some relevant spatial volume.

Table 6 lists the radionuclides that can be produced from the principle constituents in air along with the reaction mechanisms associated with their production and an estimate of the average production cross section. The large cross sections for (n,γ) and (n,p) reactions are for captures of neutrons of thermal energies while the remaining cross sections are generally the saturation cross sections found in the region above approximately a few 10's of MeV. The γ-ray induced reactions are present at virtually all accelerators and at most energies. The corresponding cross sections will be energy-dependent especially at energies just above the reaction thresholds.

Accounting for Ventilation

Adjustments for the presence of ventilation can be quite conveniently made for a given radionuclide by using an effective decay constant $\lambda'=\lambda+r$ that includes the physical decay constant λ along with a ventilation term r;

$$r = \frac{D}{V}, \quad (43)$$

with D being the ventilation rate in air volume per unit time and V being the enclosure volume. Thus r is the number of air changes per unit time. The applicable differential equation, an extension of Eq. (6) with ventilation included as a removal mechanism, is

$$\frac{dn'}{dt} = -\lambda n'(t) - rn'(t) + N\sigma\phi = -\lambda' n'(t) + N\sigma\phi \, . \quad (44)$$

After an irradiation time t_i with no initial activation, the solution is

$$n'(t_i) = \frac{N\sigma\phi}{\lambda + r}\left\{1 - \exp\left[-(\lambda + r)t_i\right]\right\} . \quad (45)$$

So the specific activity with mixing $a'(t_i)$ is

$$a'(t_i) = \lambda n'(t_i) = \frac{\lambda N\sigma\phi}{\lambda + r}\left\{1 - \exp\left[-(\lambda + r)t_i\right]\right\} . \quad (46)$$

But $N\sigma\phi$ is just the saturation concentration a_{sat} without mixing [see Eq. (9)]. Hence, with mixing the saturation concentration a'_{sat} is

$$a'_{sat} = \frac{\lambda\, a_{sat}}{\lambda + r} \, . \quad (47)$$

Since low energy accelerators must contain their beams in continuous vacuum systems, the activation of air at these machines is greatly minimized. At high energy accelerators, it is quite common to have air gaps at certain interface points to accommodate devices associated with beam targetry or beamline diagnostic instrumentation rendering continuous vacuum

impractical. These "air gaps" are only found in external beam lines and in linear accelerators. The beam in a circular accelerator or storage ring is, of necessity, contained in continuous vacuum since any air gaps traversed numerous times each second by the beam particles would destroy the beam. In addition, the large multiplicity of secondary particles produced as a part of cascade processes, either electromagnetic or hadronic, can produce airborne radioactivity external to the beamline vacuum.

If the accelerator enclosures were completely sealed, there would be no releases to the outside world and the hazard of these airborne radionuclides would be entirely restricted to those who might have to enter the enclosures. This would, however, allow the longer-lived radionuclides to build up in accord with Eq. (41). Also, ventilation is generally needed to provide cooling of components and certainly to provide fresh breathing air for workers. Typically, the average residence time of air in accelerator enclosures is limited to a range of between approximately 30 minutes and about an hour. Thus, the airborne radionuclides in the accelerator environment, in equilibrium, will have half-lives only up to the order of one hour. The residence time of the air in conjunction with the cross sections determines the radionuclides of importance. At some facilities releases of airborne radionuclides to the outdoors are minimized by greatly restricting the release rate of air during accelerator operations. When personnel accesses are made subsequent to operations, the ventilation rate must then be increased to levels consistent with good industrial hygiene practice.

Propagation of Airborne Radionuclides in the Environment

Of course the most important consideration concerning airborne radioactivity is the dose delivered to both workers in the environs of the accelerator and members of the public when radionuclides are released to the atmosphere external to the accelerator enclosure. Worker

exposure to airborne radionuclides at accelerators can be controlled to large degree by limiting or excluding access to the enclosures during operations, a practice generally needed to prevent exposure to much greater prompt radiation hazards. The control of dose receive by members of the public is connected to meteorology, usually as specified by regulatory requirements exemplified here a summary of those pertaining to U. S. Department of Energy (USDOE) facilities. Comparable requirements applicable to accelerators regulated by other agencies exist. The U. S. Environmental Protection Agency (USEPA) has placed an annual limit of 10 mrem on dose equivalent to members of the general public due to the operations of DOE facilities and has also specified on how such releases are to be measured or estimated (U. S. Code of Federal Regulations 1989). An annual dose equivalent of 10 mrem spread out throughout a one year period is difficult or impossible in practice to measure against the much larger background levels of radiation. In view of this the regulation prescribes the measurement of the activity released and the calculational model to be used to estimate the maximum dose equivalent that actual members of the public could receive. Computer modeling programs specified by the regulations are used to carry out the required calculation. A Gaussian plume model that combines input data on the release of radioactivity with meteorological information is employed. The details of such computer modeling will not be described here, but a short synopsis of analytical methods is provided to illustrate the general features and the connection to meteorology.

Due to the nature of accelerator operations, only "steady-state" conditions are considered since transient accidental releases from accelerators are unlikely. Ventilation release points are commonly called stacks. Somewhat unlike examples found at other types of facilities where radioactivity is present, release stacks at accelerators are in generally not very tall. The radionuclide concentration $\overline{c}\ (x,y,z)$ (Bq m^{-3}) as a function of Cartesian coordinates (x,y,z) (all in

meters) is given by Sutton's equation (Slade 1968);

$$\bar{c}(x,y,z) = \frac{Q}{2\pi\sigma_y(x)\sigma_z(x)\bar{u}}\left\{\exp\left[-\frac{\lambda}{\bar{u}}\sqrt{x^2+y^2}\right]\right\}$$
$$\times\left\{\exp\left(-\frac{y^2}{2\sigma_y^2(x)}\right)\right\}\left\{\exp\left[-\frac{(z-h)^2}{2\sigma_z^2(x)}\right]+\exp\left[-\frac{(z+h)^2}{2\sigma_z^2(x)}\right]\right\}. \quad (48)$$

In this equation (x,y,z) are measured at a point of interest from the foot of the stack where x is along the centerline of the plume as determined by the wind direction (downwind), y is the transverse coordinate, and z is the vertical coordinate. Q is the emission rate of (activity s^{-1}) and $\bar{u}$ is the mean wind speed (meters s^{-1}). $\sigma_y(x)$ and $\sigma_z(x)$ are dispersion coefficients that are functions of the downwind coordinate x. The exponential involving the decay constant λ conservatively allows for radioactive decay in transit for a particular radionuclide. h is the effective chimney height, different than the physical chimney height h_a if the velocity of the expelled air is significant. h is determined from

$$h = h_a + d\left(\frac{v}{\bar{u}}\right)^{1.4}\left(1+\frac{\Delta T}{T}\right). \quad (49)$$

In Eq. (49) d is the outlet diameter (meters), v is the exit velocity of the gas (meters s^{-1}), and $\Delta T/T$ is the relative difference between the absolute temperature of the gas ΔT and the ambient outdoor temperature T. For the common situation of interest where the receptor location of concern is at ground level (z=0), Eq. (48) becomes

$$\bar{c}(x,y,0) = \frac{Q}{\pi\sigma_y(x)\sigma_z(x)\bar{u}}\left\{\exp\left[-\frac{\lambda}{\bar{u}}\sqrt{x^2+y^2}\right]\right\}\left\{\exp\left[-\left(\frac{y^2}{2\sigma_y^2(x)}+\frac{h^2}{2\sigma_z^2(x)}\right)\right]\right\}, \quad (50)$$

taking into account the presence of the ground as a reflecctive “barrier”. Important parameters in these equations are determined by the meteorological conditions.

Table 7 provides a classification of the meteorological conditions to be used in Sutton’s

Equation. Following determination of the dominant meteorological condition, the values of $\sigma_y(x)$ and $\sigma_z(x)$ can be read off of Figs. 14 and Fig. 15, respectively and the results used to evaluate the applicable version of Eqs. (48) or (50).

Airborne radioactivity releases can be minimized by limiting the ventilation rates during operations when people are not present in the enclosure, delaying the actual emissions by requiring long pathways to the ventilation "stacks", or minimizing air gaps in the beam.

Radiation Protection Standards for Airborne Radioactivity

Airborne radioactivity is of primary concern to workers who might enter an accelerator enclosure to perform maintenance activities; thus classified as "occupational workers". Since the principal radionuclides are of relative short half-life, the hazard is largely due to the “immersion” in a “cloud” of external dose rather than a gaseous ingestion hazard such as might be found in operations involving the processing of long-lived radioactive materials where uptakes having lengthy biological half-lives must be taken into account. Regulatory authorities, guided by recommendations of the International Commission on Radiation Protection (ICRP) and National Council on Radiation Protection and Measurements (NCRP) have established Derived Air Concentrations (DACs) for radiation workers. The values of the DACs are based upon the receipt of 50 mSv (5 rem) of dose equivalent by an individual if the entire employment year (≈ 2000 hours, or 40 hours weekly) is spent working in a concentration corresponding to 1.0 DAC. Concentrations approaching those as large as one DAC are only very rarely encountered in accelerator radiation environments. Similarly, for members of the general public, values of Derived Concentration Guides (DCGs) have been tabulated that correspond to the receipt of 1 mSv (100 mrem) of dose equivalent by an individual who spent all of the time in one year breathing such air. Table 8 gives representative values of these circumstance-dependent

maximum concentrations $C_{max,i}$ for individual accelerator-produced radionuclides in air based upon present USDOE (U. S. Department of Energy 1990, U. S. Code of Federal Regulations 1998) along with companion values determined for accelerator-produced radionuclides not included in the cited references as calculated by Hoefert (1969). For some radionuclides commonly found at accelerators, the regulations cited gives two values of DAC, one for air inhaled into the lungs and the other for immersion in an infinite cloud of γ-emitting radionuclides. Since these concentration limits can represent legal requirements, the authority having jurisdiction should be consulted in their use. In general the most restrictive values are listed. At the time of writing this chapter, USDOE issued a revision to its regulations that will need to be implemented by 9 July 2010 (U. S. Code of Federal Regulations 2007). Parts of Table 8 will need to be modified by full implementation of this revision to the regulations.

Immersion conditions are more likely to be the dominant exposure mechanism due to activated air at accelerators. However, for occupational exposures, the sizes of the "clouds" are not likely to be "infinite", instead determined by the dimensions of the accelerator enclosures. Hoefert's calculations are thus useful in the proper evaluation of workplace conditions since under immersion conditions, the dose received by an individual strongly depends on the size of the cloud. Clouds of infinite extent are rare inside buildings at accelerators. Hoefert calculated the equivalent of DACs for clouds of various sizes. Table 8 gives those for clouds of 4.0 meters radius that are plausibly typical of an accelerator enclosure. For the general population, the choice of an infinite cloud is appropriate, since such exposure would presumably occur outdoors.

Mixtures of radionuclides are commonly encountered. To account for the presence of multiple radionuclides, the set of individual radionuclide concentrations in the air C_i must satisfy

$$\sum_i \frac{C_i}{C_{\max,i}} \le 1, \quad (51)$$

where $C_{max,i}$ is the regulatory standard for the i^{th} radionuclide, appropriate for the circumstances of the exposure (e.g., worker, member of the public).

Production of Airborne Radionuclides at Electron Accelerators

At electron accelerators, as with activation of accelerator components, significant air activation will not occur without bremsstrahlung since the nuclear cross sections of electrons are about two orders of magnitude smaller than are those of photons. This airborne radioactivity is generally short-lived and the concentrations, as shall be seen shortly, are usually quickly reduced to levels where the the absorbed dose rates are small compared to those due to the performance of work near the accelerator components. This result reflects the fact that the radiation length of air is so much longer than that of any solid material. Swanson (1979a) has calculated the saturation activities produced in air normalized to the electron beam power with the results provided in Table 9. The results of these calculations are normalized to unit path length and to beam power. To use them to determine the volume specific activity (e.g., GBq cm^{-3}) in a given accelerator enclosure, one must multiply the tabulated values by the available bremsstrahlung path length and divide by the enclosure volume. The bremsstrahlung path length is set either by the physical dimensions of the room or by the attenuation length of the bremsstrahlung radiation in air. For energies close to the threshold of an individual reaction, the rise of activity with beam energy E_o must be understood. ^{41}Ar is produced in the thermal neutron capture reaction $^{40}Ar(n,\gamma)^{41}Ar$ most copiously where there are high fluences of moderated neutrons present, typically near water-cooled targets and in concrete enclosures. ^{3}H, ^{14}C, and ^{7}Be are too long-lived to be produced at levels anywhere near saturation. After calculating the production rates, one can determine the concentrations within the accelerator enclosure and estimate the effective dose equivalent rates at offsite locations as well as the compliance with applicable regulations.

Production of Airborne Radionuclides at Proton Accelerators

At proton accelerators, the excitation functions of the possible nuclear reactions are important as exemplified in Fig. 4. In general, the positron emitters ^{11}C, ^{13}N, ^{15}O, along with ^{41}Ar (here also produced by thermal neutron capture), are the nuclides most frequently seen. Work at Fermilab described by Butala et al. (1989) and Vaziri et al. (1993 and 1996) has also confirmed these identifications and, additionally, detected ^{38}Cl and ^{39}Cl. The determination of the relative contributions of the various positron emitters present must principally be done by fitting measured decay curves (i.e., with a multi-channel scaler) with a sum of exponential functions, each term of which represents one of the possible radionuclides present. This reflects the fact that their γ-ray spectra are all dominated by 0.511 MeV photons from positron annihilation, without a unique γ-ray decay signature other than the half-lives. In addition, the production of ^{3}H in the molecular form HTO and its impact should be evaluated.

It was concluded by Butala et al. (1989) that the geometry of target stations significantly can affect the composition. For example, high intensity targets immediately surrounded with large volumes of iron in contact with a surrounding layer of concrete produced much less ^{41}Ar than did other targets where the bulk iron shield was located in a open room with an air space between the iron and the concrete walls. Presumably, the open space provided opportunity for the large flux of low energy neutrons expected external to a pure iron shield to "thermalize" and thus enhance the production of ^{41}Ar in the air space given the large cross section of the $^{40}Ar(n,\gamma)^{41}Ar$ reaction at thermal neutron energies (σ_{th}=660 mb at E_n=0.025 eV). The photons emitted as a result of this and other neutron capture reactions also may initiate the (γ,p) and (γ,pn) reactions required to produce significant quantities of ^{39}Cl and ^{38}Cl, respectively. Some typical percentages of the various radionuclides, by activity concentration, released from high

energy proton accelerators are given in Table 10.

After calculating the production rates, one can then apply the general methodology presented in this chapter to estimate the effective dose equivalent rates and assure regulatory compliance.

Water and Geological Media Activation

The condition of groundwater resources is a significant public concern that includes the need to assure protection of such valuable resources from contamination with radionuclides. Radioactivity can be produced in soil or rock and in the water it contains. Sometimes the radioactivity produced in water is a matter of concern for occupational workers as well. In practice, it is not always a simple matter to separate these two regimes. One can, in principle, initiate calculations of groundwater activation at accelerators by starting from "first principles" and by using the activation equation (Eq. (10).

Water Activation at Electron Accelerators

As seen before, questions of radioactivation are generally less complex at electron accelerators. As was done for atmospheric radioactivation, Swanson (1979a) has provided the results of calculations to address the production of radionuclides in water at electron accelerators. Such activation will principally occur in water used to cool magnets and beam absorbers and can become a radioactive waste issue. The results are, again, in the form of saturation activities normalized to the electron beam power absorbed in the water volume. Such activities, as before, are for infinite irradiation periods with no time allowed for decay. The results are given in Table 11, that also includes the point source specific gamma-ray constants Γ useful for calculating absorbed dose rates near such water and the radionuclide production cross section per MeV of beam energy σ. The results in this table assume that all of the beam power will be absorbed in

the water. Production of tritium will be less in situations where the beam absorber is water-cooled metal, given the space occupied by the metal. These results will be reduced by large factors at low energies near the reaction thresholds. From these results, it is clear that, aside from short-lived positron emitters, only ^{3}H and ^{7}Be are of importance. These are produced by interactions with the oxygen, 99.76% of which is ^{16}O, found in water. Activity concentrations are usually obtained by assuming rapid mixing of the saturated activity in the available volume of water. In principle, ^{3}H could be produced from the hydrogen in water by means of the two sequential thermal neutron capture reactions, $^{1}H(n,\gamma)^{2}H$ followed by $^{2}H(n,\gamma)^{3}H$. However this is unimportant due to the fact that the cross sections for both thermal capture reactions involved are fractions of a millibarn. It should be recognized that tritium in the form of HTO vapor molecules can, under favorable conditions of temperature and relative humidity, be condensed as liquid water in an enclosure, thus transforming "air" activation into water activation.

At electron accelerators, the bulk shielding scales with the radiation length, a quantity that for materials having atomic number greater than three is smaller, often much smaller, than the nuclear interaction length characteristic of hadron shielding. This makes the bulk shielding of electron accelerators much more compact compared with that at proton and ion accelerators. The result is that soil activation is generally a less important issue at electron machines.

Water and Geological Media Activation at Proton Accelerators

Water Activation. At proton and ion accelerators, as with electron accelerators, radioactivity can be produced directly in water as a result of both proton and neutron interactions. Values for some of the relevant cross sections were given in earlier. Equipped with knowledge of the beam energy and information about the energy spectra of neutrons that are present, one can proceed to calculate the activity produced. In general, the most important

radionuclides, as is the situation with electron accelerators, result from the interactions of the hadrons with the oxygen present in the water. The production of ^{3}H in water from atoms other than hydrogen is of special importance. As before, the production of ^{3}H from the hydrogen present in the water is possible, but is rendered sufficiently improbable due to the small cross sections of the two thermal neutron capture reactions required to occur sequentially. Konobeyev and Korovin (1993) have developed a global fit to the existing cross section data on the production of ^{3}H due to neutron interactions with a variety of target elements found in soils with the results shown in Fig. 16. The results for incident protons are similar. Again, it should be recognized that tritium in the form of HTO vapor molecules can, under favorable conditions of temperature and relative humidity, be condensed as liquid water in an enclosure, thus transforming "air" activation into water activation.

Geological Media Activation. While calculating the production of radionuclides in soil, and in the water it contains, directly from known cross sections is appealing due to its simplicity, in practice such calculations have been done more frequently by analyzing results obtained using irradiated samples. The work of Borak et al. (1972) is of singular importance in this regard. Borak et al. measured the radioactivity produced in soil by high energy hadrons using radiochemical analysis of soil samples irradiated near high energy synchrotrons; the dismantled 12 GeV Zero Gradient Synchrotron (ZGS) at Argonne National Laboratory (ANL) and the 28 GeV Alternating Gradient Synchrotron (AGS) at Brookhaven National Laboratory (BNL). The radionuclides ^{3}H, ^{7}Be, ^{22}Na, ^{45}Ca, ^{46}Sc, ^{48}V, ^{51}Cr, ^{54}Mn, ^{55}Fe, ^{59}Fe, and ^{60}Co were identified. Only radionuclides with half- lives exceeding 15 days were considered.

Experiments were then performed to determine which radionuclides, and what fractions of them, could be leached by water. This study determined macroscopic production cross

sections and ion velocities relative to ground water flow in soil. Of these nuclides only ^{3}H, ^{22}Na, ^{45}Ca, and ^{54}Mn were observed in leach waters. All ^{3}H in the form of HTO was assumed to be leachable and was measured by driving it out of the sample by baking. The results were based upon the elemental composition of soil given in Table 12. Borak et al. measured specific activities at saturation A_i (Bq g^{-1}) that are related to the microscopic cross sections by means of the following equation:

$$A_i = \phi \sum_j n_j \sigma_{ij} \quad ,(52)$$

where ϕ is the flux density (cm^{-2} s^{-1}), n_j is the number density of target nuclei of the j^{th} nuclide (g^{-1}) of the soil sample, and σ_{ij} (cm^2) is the effective cross section for the transformation from target nucleus *j* to radionuclide *i*. The summation is taken over the soil constituents. Borak et al. directly measured the summations on the right hand side of Eq (52). These summations over the individual soil constituents for each radionuclide of interest represent the total macroscopic cross sections. Table 13 gives the results of the measurements of these, denoted Σ (cm^2 g^{-1}), for each of the radionuclides identified in the various soils analyzed.

Borak et al. also obtained data related to the leachabilities of the various elements from the soils studied. Leachability measures the ability of water to remove a given radionuclide from the soil material. It is not related to properties of the nucleus, rather it is a chemical process including ion exchange. The results reported by Borak et al. will now be given.

For ^{3}H the leaching process was able to collect all the tritium as measured by a bake-out process. The average value of the macroscopic cross section in soil was found to be 5.1×10^{-3} cm^2 g^{-1} of water. An important conclusion is that the tritium will migrate with the same velocity as any other water in the soil.

For ^{22}Na, typically 10-20 % of this nuclide was found to be leachable. On average, it appeared that the migration velocity of this nuclide is approximately 40% of that of water through the soil due to ion exchange processes.

For ^{45}Ca, at most 5 % of this nuclide was leached from the soil. The migration velocity was determined to be extremely small.

For ^{54}Mn, at most 2 % of this nuclide was leached from the soil. It was determined that this nuclide will not migrate significant distances.

Thus, based upon leachability considerations, ^{3}H and ^{22}Na are the most important leachable radionuclides that can be produced in environmental media such as soil.

One can thus calculate the quantities of radionuclides that might pose a risk to groundwater in the environs of an accelerator. This can be done by using the cross sections directly, or, as demonstrated by Gollon (1978), by performing Monte Carlo calculations to deterimine the total stars (i.e., the total inelastic nuclear interactions above some threshold) produced in some volume of earth shielding. As in Eq. (35), the total number of atoms P_i of the i^{th} nuclide that can be produced per star in that same volume is given by

$$P_i = \frac{\Sigma_i}{\Sigma_{in}}, \quad (53)$$

where Σ_i is, as above, the macroscopic cross section (cm^2 g^{-1}) for the i^{th} radionuclide in soil and Σ_{in} is the total macroscopic inelastic cross section (cm^2 g^{-1}) for soil. Gollon inferred a value of Σ_{in}=1.1x10^{-2} cm2 g^{-1} for soil from the results of Borak et al. (1972). Modern Monte Carlo codes can now calculate these quantities directly from energy-dependent corss sections stored in a database. However, given the limited energy dependence at high energies, working with the total stars remains worthwhile as a means to achieve results rapidly. This method can also serve as a

quality check on more complex calculations.

Gollon used the following values of P_3 for ^{3}H and P_{22} for ^{22}Na selected from the paper by Borak et al. (1972) for soils found in glacial till at Fermilab and used here as an example:

$$P_3 = \frac{8.2\times10^{-4}}{1.1\times10^{-2}} = 0.075 \text{ , and (54a)}$$

$$P_{22} = \frac{2.1\times10^{-4}}{1.1\times10^{-2}} = 0.020 \text{ .(54b)}$$

One can then calculate the total number of atoms of radionuclides produced during some time interval in some volume by simply multiplying these factors by the number of stars (i.e., inelastic interactions) in the same volume. The number of atoms then can be converted to activity by multiplying by the decay constant [Eq. (3)]. For a specific soil or rock composition, one should use cross sections for producing the radionuclides of interest in each of the chemical elements present, integrate over the energy spectrum of incident hadrons, and finally take a summation over the individual component elements. Fig. 17 gives microscopic cross sections for producing ^{22}Na by interactions of hadrons with the various elements comprising soil as tabulated by Van Ginneken (1971). This figure can be viewed as a companion to Fig 16.

Regulatory Standards. The quantity of ultimate concern, of course, is the resultant concentration in water. The water could be an actual or potential drinking water resource that might be subject to specific regulatory requirements. The regulations may differ between governing jurisdictions. The requirements, generally not developed for application to the operations of particle accelerators, need to be understood by facility management personnel. The standards can differ for drinking water supplies and surface water discharges. The allowable concentrations for surface waters may be larger due to the likelihood that such discharges will most certainly be diluted significantly prior to the consumption by individuals. However, in

some jurisdictions, this may not be the case. For public drinking water supplies, the U. S. Environmental Protection Agency (USEPA) (U. S. Code of Federal Regulations 2000) limits such concentrations to those that would produce a postulated annual dose equivalent of 4.0 mrem with a specific limit of 20 pCi cm^{-3} ($7.4x10^5$ Bq m^{-3}) for tritium in the form of HTO. (The value is given in customary units first because it is the applicable standard, given in those units, by the referenced regulation. The second quanity is a calculated conversion to SI units performed by this author for comparison purposes only.)

An explicit limit for ^{22}Na is not specified by USEPA. For surface water discharges, the USDOE (1990) has set forth Derived Concentration Guides (DCGs); values of concentrations that would result in members of the public each receiving no more than 1.0 mSv in a given year should they use such water for their household needs on an ongoing basis. The DCGs are based upon a more up-to-date dosimetry methodology that results in values of 80 pCi cm^{-3} ($3x10^6$ Bq m^{-3}) for ^3H and 0.4 pCi cm^{-3} ($1.5x10^4$ Bq m^{-3}) for ^{22}Na in drinking water. However, the USEPA explicit limit for ^3H in drinking water, based upon obsolete ICRP methodology, is considered legally preeminent, retained because it is more protective of members of the public. For purposes of this discussion, surface water discharges include those to streams, ponds, etc. while drinking water standards apply to water that could potentially end up in a source of drinking water such as a public, or even private, well. Local jurisdictions can, and have, applied drinking water standards to all discharges including surface ones, especially in situations where a surface water feature such as a pond or stream is utilized directly as a source of drinking water. For surface water discharges not considered to be to waters representing drinking water supplies, the respective DCG values for HTO are 2000 pCi cm^{-3} (7.4×10^7 Bq m^{-3}) and for ^{22}Na are 10 pCi cm^{-3} (3.7×10^5 Bq m^{-3}).

As with airborne radioactivity, these limiting values for individual radionuclides $C_{max,i}$ are to be used in Eq. (51) for exposure to water where multiple radionuclides with individual concentrations C_i are present.

The Propagation of Radionuclides in Geological Media

The methods for calculating these concentrations in actual environmental media will vary with the regulatory authority and the "conservatism" of the institution. The most conservative assumption is to assume that saturation concentration values of production are reached. This is equivalent to assuming that the accelerator will operate “forever” in a static configuration and that the water in its vicinity never moves. This assumption is extremely unrealistic as such "motionless" water in such a medium hardly comprises a viable source of useable drinking water. For an irradiation over a finite period of time, the activity concentration C_i of radionuclide i in leaching water under such conditions can be calculated by means of following formula:

$$C_i = \frac{N_p P_i L_i S_{ave}}{31.62 \rho w_i} \{1 - \exp(-t_{irrad} / \tau_i)\} \exp(-t_c / \tau_i) \text{ (Bq m}^{-3}\text{)}, (55)$$

where N_p is the number if incident particles delivered per year, P_i is as above, L_i is the fraction of the radionuclide of interest that is leachable, S_{ave} is the average star density (stars cm^{-3}) in the volume of interest per incident particle, ρ is the density of the medium (g cm^{-3}), and w_i is the mass (grams) of water per unit mass (grams) of medium required to leach some specified fraction of the leachable radioactivity. The quantity w_i thus linked to the value of L_i. t_{irrad} is the irradiation time, t_c is the “cooling” time once the irradiation is suspended, and τ_i is the mean-life of the i^{th} radionuclide. The constant in the denominator contains the unit conversions needed to yield results in Bq m^{-3}. It has a value of 1.17 x 10^6 if one desires the concentration on pCi cm^{-3} with all other quantities in these same units. For a given medium, the ratio L_i/w_i should be

determined by measurements specific to the local media.

An important quantity is the effective porosity p, the volume fraction of the material that is available to water movement, connected with the density of the media ρ (g cm^{-3});

$$p = \rho w_i \quad (56)$$

The effective porosity is essentially equal to the pore volume of the material in a unit volume of soil but for consolidated materials (i.e., rock) it does not include sealed pores through which water movement does not occur. Porosity values vary considerably but in general are in the range of $0.2<p<0.35$. The above methodology provides a means for making "worst case" estimates. For realistic estimates water movement must be taken into account.

At Fermilab, a simple model allowing for some movement and further dilution of water was employed for many years (Gollon 1978). In this single resident model for reasons that are obvious, the vertical migration of water was assumed to be 2.2 m yr^{-1}. In the clay soils typical of the Fermilab site, this velocity is very conservative, likely large by at least an order of magnitude. Its use, rather crudely, allowed for the presence of cracks and fissures, and even "sand lenses", through which more rapid propagation of water would be possible. The vertical velocity for HTO was taken to have this value while the results of Borak et al. (1972) inferred a value of about 1.0 m yr^{-1} for ^{22}Na. Only the leachable fraction of the ^{22}Na was included.

The procedure allowed for decay during the downward migration of the total inventory of radionuclides produced in one year, integrated over the entire volume of the irradiated material, to the highest aquifer below the location of the irradiation. At that point, it was assumed that the radionuclides were rapidly (i.e., with no allowance for radioactive decay) transported horizontally to a shallow well where it was presumed that the flow of water collecting the radionuclides is entirely used by an individual user who consumes a volume of 0.15 m^3 per day.

This value, a minimal one, was taken from results achieved by municipalities that have needed to ration public water consumption during conditions of severe drought. Thus the annual production, as transported vertically, was diluted into the 55 m^3 yr^{-1} that this represents. This simple model is generally conservative but it does neglect that fact that the water movement may not be uniform from year-to-year. It also did not take advantage of the fact that the radionuclides are initially distributed over a considerable volume during production. This provides an intrinsic initial dilution into a finite; an important feature given the absence of any mechanisms for increasing the concentration.

It is clear that better methods are warranted and a better model has been developed for use at Fermilab (Malensek et al. 1993). This concentration model calculates the production of the radionuclides of concern in accordance with Eq. (55). Variations of this approach are used at other accelerators, as well. The result provides an initial concentration that is available for further migration, decay, and dilution. The concentration subsequent to migration is calculated using up-to-date modeling techniques to determine the reduction in the concentration due to dilution, diffusion, and radioactive decay. Advantage was taken of modeling techniques developed to design sanitary landfills to prevent migration of contaminants to groundwater resources, with radioactive decay added in for this special application. At a point of interest, typically an aquifer serving as a potential or actual supply of drinking water, the concentrations are calculated with these techniques and then substituted in Eq. (51) in order to determine the adequacy of a given shielding design.

To perform such calculations properly requires some knowledge of hydrogeology with a summary of the basic principles given here. Groundwater physics has been discussed at length in several of the references (Fetter 1988; Batu 1998). A recent concise summary of the topic from a

physicist viewpoint has been provided by Anderson (2007). In situations where a definite potential gradient called the hydraulic gradient *dh/dx* is applied to water in a medium, the rate of flow is said to be advective. Under such conditions and in situations where only one dimensional coordinate is important, the average linear velocity (usually the vertical seepage velocity) *v* is given by the application of Darcy's Law (Fetter 1988);

$$v = \frac{K}{p}\frac{dh}{dx}, \quad (57)$$

where *p* is, as expected, the effective porosity. More complicated situations involving two and three dimensions are addressable using the mathematical language of vector calculus. The derivative in Eq. (57) is the gradient of the hydraulic head in the material. *K* is the hydraulic conductivity**.** This quantity is a function of the material and its moisture content. All of the factors in this equation can, and generally should, be determined empirically for the medium and location under consideration. Typical values of *K* are given in Table 14 (Batu 1998).

Darcy's Law can, then, be used to determine the rate of migration of a contaminant, in this case radioactivity, from one point to another. During the time of migration, the concentration would be decreased by radioactive decay while possibly being increased by any ongoing radioactivation while in transit. One often encounters the problem of calculating the concentration of radionuclides at some location as a function of time during, or after, a period of irradiation comparable to the mean-lives of the radionuclides of concerns. At a given location in such a medium denoted by the coordinate *x*, one needs to solve the following continuity equation that can be thought of as an extension of Eq. (6), if the velocity of water movement *v* can be thought of as slowly varying or a constant over time *t* and some volume of space:

$$\frac{\partial C_i}{\partial t} + v\frac{\partial C_i}{\partial x} + \lambda_i C_i(x,t) = \frac{L_i}{w_i'} Q_i(x,t), \quad (58)$$

where all variables are as in Eq. (55) with the refinements that λ_i is the decay constant of the i^{th} radionuclide, x is the spatial coordinate, and w_i' is the water content of the media per unit volume of media*. The quantity $Q_i(x,t)$ represents the production of the i^{th} radionuclide and is equivalent to the factor $N_p S_{ave}/(31.62\rho)$ in Eq. (55). It includes any time-dependence in the delivery of beam. The middle term in the left-hand side of the equation takes care of movement from a point of one concentration to another at the seepage velocity v. In many situations in a shielding medium, one can commonly describe the spatial dependence of the production factor as an exponential function, so in those situations one has

$$Q_i(x,t) = Q_{oi}(t)\exp(-\xi x) \quad (59)$$

For the typical initial conditions of $C_i(x,0)=0$ and $x \geq 0$, $t \geq 0$ this has the analytical solution;

$$C_i(x,t) = \frac{L_i}{w_i}\int_0^t dt' Q_i(x - vt', t')\exp(-\lambda t') \quad (60)$$

For the exponential dependence applied in Eq. (59) this becomes:

$$C_i(x,t) = Q_{oi}(t)\frac{L_i}{w_i}\frac{1}{\eta_i}\exp(-\xi x)[\exp(\eta_i \tau) - 1] \quad (61)$$

with $\eta_i = \xi v - \lambda_i$, $\tau = t$ for $t < x/v$, and $\tau = x/v$ for $t \geq x/v$ $C_i(x,t)$ has a maximum at $x_{i,\max}$ given by

$$x_{i,\max} = -\frac{v}{\lambda_i}\frac{\ln\left(\frac{\xi v}{\lambda_i}\right)}{1 - \frac{\xi v}{\lambda_i}} \quad (62)$$

In using these results, one must take care that the algebraic signs of the coordinates x relative to that of v are properly taken into account. In situations where the seepage velocity is extremely slow, diffusion becomes the dominant mechanism for water flow and dilution. Mathematically, a

* This solution is due to N. V. Mokhov, private communication (1997).

second partial derivative with respect to the spatial coordinate is added to Eq. (58). Examples are provided by Fetter (1988). Computer codes has been written to address this topic such as the one produced by Sudicky et al. (1998).

As a further example of methodologies that can be employed in solving such problems, Jackson et al. (1987) have estimated the dilution for a shallow uncased well in an aquifer a distance *r* from a beam loss point also in the aquifer. The loss point was assumed to be within the cone of influence (i.e., the drawdown zone) of the well. This was performed for a simple geology that involved a single uniform stratum of earth above some level of impervious stratum. Fig. 18 shows the situation described by this model where a given well is modeled by using the profile of the depth of water $h(r)$, as a function of r. $h(r)$ is determined by the depth of a test well at radius r from the well under consideration and represents the hydraulic potential. The well is assumed to supply a volume Q of water per day. The flux of water is determined by an equivalent of Darcy's Law;

$$S_r = k\frac{dh(r)}{dr}, \quad (63)$$

where S_r is the inward flux at radius r and k is a constant with dimensions of volume per unit time per unit area, that is characteristic of the medium. Conservation and incompressibility of water yields

$$Q = 2\pi r h(r) S_r = 2\pi r k h\frac{dh}{dr} = \pi k\frac{d(h^2)}{d(\ln r)}. \quad (64)$$

The quantity $2\pi rhdh/dr$ corresponds to the rate of change of volume of the cylindrical shell of height h (i.e., the hydraulic head) with respect to r. Eq, (64) has the solution;

$$Q\ln\left(\frac{r}{r_o}\right) = \pi k\left\{h^2(r) - h_o^2\right\}, \quad (65)$$

where r_o is the radius of the well and h_o is the height of water above the impervious stratum at the well. If H is the depth of the impervious layer below the water table in an asymptotic region unperturbed by any wells, the radius of influence R of the well can be defined by the relation;

$$\ln\frac{R}{r_o}=\frac{\pi k\left\{H^2-h_o^2\right\}}{Q}\ .(66)$$

However, the detailed solution is not necessary. Suppose that there is a well a distance r away from the region of deposition of radioactivity near an accelerator. One might also assume that the activation zone lies below the water table and that the deposition region lies within the radius of influence of the well. This assumption is "conservative" because it leads to higher concentrations than would be obtained if the activation zone were totally, or partially, above the water table. The amount of activity drawn into the well is determined by the rate of pumping Q and the necessary total flow through a cylinder of radius r and height $h(r)$ as we have seen. Let ΔV be the volume of soil yielding Q gallons of water. The cylindrical shell providing this amount of water will be of radial thickness Δr, where $\Delta V=2\pi rh(r)\Delta r$. If $\Delta r<t$, the fraction F of the volume of activity included in this shell can be said to be given by

$$F=\frac{\Delta r}{t}=\frac{2\pi\ rh\Delta r}{2\pi\ rht}=\frac{\Delta V}{2\pi\ rht}\ .(67)$$

If the activated region contains leachable activity A (either total activity or that of a particular radionuclide of interest), the corresponding specific activity a in water drawn from the well is

$$a=F\frac{A}{Q}=F\frac{A}{p\Delta V}=\left[\frac{\Delta V}{2\pi\ r\ h\ t}\right]\frac{1}{p}\left[\frac{1}{\Delta V}\right]A=\frac{1}{2\pi\ r\ t\ D}\frac{f}{p}A\ ,(68)$$

where $f=D/h$ is the fraction of the total height of the cylindrical shell occupied by the activated region and p is the effective porosity of the soil. The pumping volume Q is implicit in f.

Thus, this formula may be used to obtain an estimate of the specific activity as a function

of distance from the well, although it is perhaps not too useful for applications to beam losses far from the well. By definition, $f \leq 1$ and a minimal value of porosity can be used to obtain upper limit estimates of the concentration. It must be emphasized that this model depends upon uniformity of water conduction by the strata. The presence of cracks, voids, so-called "sand lenses will, of course, provide much more rapid movement that is not well-described by this simple model. On the other hand, strata of solid rock will provide slower movements of the radioactivity.

Activation Detectors

In a discussion of the production of radioactivity at accelerators, it would be remiss to not mention its use as an "instrumentation" technique. Certain nuclear reactions have relatively sharp thresholds which can be used to determine portions of a hadron spectrum that exceed it since the "leveling off" of the cross sections are often well-behaved. Table 15 summarizes some of the useful reactions along with some pertinent information about threshold detectors that have been found to be useful in practical work. Some of these reactions will be discussed further here. There are other lists of useable threshold reactions (Thomas and Stevenson 1985, 1988).

The group of reactions that produce ^{11}C from ^{12}C is of special interest because of the fact that plastic scintillators can themselves become activated by hadrons, including neutrons and protons, with kinetic energies above 20 MeV. This technique was first developed by McCaslin (1960). The cross sections for production of ^{11}C, as initiated by several different types of incident particles, are shown in Fig. 19. Stevenson (1984) has determined that a value of 28 fSv m^2 (2.8×10^{-4} μSv cm^2) is an appropriate factor to apply to the conversion of the measured fluence of neutrons with E_n>20 MeV to the dose equivalent due to those energetic neutrons. This assumes a typical accelerator spectrum found within thick shields of earth or concrete where neutrons

clearly dominate. Such measurements can be useful to determine the contribution of the high energy (E_n>20 MeV) neutrons to the total neutron dose equivalent. Moritz (1989) has found that the use of a common scintillator, NE102A (product of Saint-Gobain Crystals & Detectors, formerly Nuclear Enterprises) activated by the reaction $^{12}C(n,2n)^{11}C$ can be included as an additional high energy detector in a Bonner sphere measurement (Bramblett et al. 1970) in order to extend the energy range. Moritz, following Stevenson, used an average cross section of 22 mb for the $^{12}C(n,2n)^{11}C$ reaction. NE102A, a rather typical plastic scintillator, has a carbon content of $4.92x10^{22}$ atoms g^{-1} and a density of 1.032 g cm^{-3} (Knoll 2000). Moritz used a cylindrical detector 0.05 m in diameter by 0.05 m long and achieved an efficiency of 93 % in detecting the 0.511 annihilation γ-rays resulting from the decay of ^{11}C. The addition of this reaction reduced the degeneracy of the spectrum unfolding process inherent in the Bonner sphere technique.

Fig. 20 provides the excitation functions of some other useful reactions with very high thresholds, potentially useful for cleanly detecting high energy hadrons. The Hg→^{149}Tb reaction is a suitable monitor for very high energy particles and is commonly used as a beam calibrator. However, it has been found by Baker et al. (1984 and 1991) that there are three reactions involving copper targets that are more useful for this purpose because they produce radionuclides with half-lives longer than the somewhat inconveniently short half- life of ^{149}Tb (4.1 hr). These cross sections, include in Table 15, have been measured for energies from 30 to 800 GeV.

As is well known, ^{233}U, ^{235}U, and ^{239}Pu all have relatively large fission cross sections at low neutron energies. The *Q*-values are very large (approximately 200 MeV) so that huge output signals result. For higher energy "fast" neutrons, fission reactions become possible for other, lighter nuclei such as bismuth. The cross sections for fast neutrons of these reactions are shown in Fig. 21. Fission reactions have been exploited as neutron (or hadron) detectors at accelerators.

The fission of ^{209}Bi is especially interesting since this reaction has a threshold of about 50 MeV and also exhibits evidence that the neutron and proton-induced fission cross sections are approximately equal. Bismuth has been employed in ionization chambers where the large energy deposited by the fission fragments gives a clear "signature" of this process. Like the use of ^{11}C, it can provide further information about high energy neutrons and resolve ambiguities in the unfolding of spectra from Bonner sphere data. McCaslin et.al. (1968) have summarized some interesting results obtained using this process.

Acknowledgements

This work is adapted from lectures given by the author at sessions of the U. S. Particle Accelerator School (USPAS) on multiple occasions (Cossairt 2007). The author has benefited greatly from comments provided over the years by many colleagues. Those offered by Drs. Kamran Vaziri (Fermilab), Alexander Elwyn (Fermilab, retired), and Sayed Rokni (SLAC) have been especially helpful. The continued support of this work by Mr. William Griffing (Fermilab) is most appreciated. Most of all, I thank my wife Claudia for her encouragement and her patience with a considerable amount of work done at home.

References

Anderson MP. Introducing groundwater physics. Phys Today May:42-47; 2007.

Armstrong TW, Alsmiller Jr RG. Calculation of the resident photon dose rate around high energy accelerators. Nucl Sci Eng 38:53-62; 1969.

Armstrong TW, Barish J. Calculation of the residual photon dose rate due to the activation of concrete by neutrons from a 3-GeV proton beam in iron. In: Proceedings of the second international conference on accelerator radiation dosimetry and experience. Stanford, CA: U. S. Atomic Energy Commission CONF-691101; 1969: 70-91.

Barbier M. Induced radioactivity. Amsterdam: North-Holland Publishing Company; 1969.

Batu V. Aquifer hydraulics. NewYork, NY: John Wiley and Sons, Inc.; 1998.

Baker SI, Kerns CR, Pordes SH, Cumming JB, Soukas A, Agoritsas V, Stevenson GR. Absolute cross section for the production of ^{24}Na in Cu by 400 GeV protons. Nucl Instrum and Meth A222:467-473; 1984.

Baker SI, Allen RA, Yurista P, Agoritsas V, Cumming J**.** Cu(p, x)^{24}Na cross section from 30 to 800 GeV. Phys Rev C43:2862-2865; 1991.

Borak TB, Awschalom M, Fairman W, Iwami F, Sedlet J. The underground migration of radionuclides produced in soil near high energy proton accelerators. Health Phys 23:679-687; 1972.

Bramblett RL, Ewing RI, Bonner TW. A new type of neutron dosimeter. Nucl Instrum and Meth 9:1-12; 1960.

Butala SW, Baker SI, Yurista PM. Measurements of radioactive gaseous releases to air from target halls at a high-energy proton accelerator. Health Phys 57:909-916; 1989.

Cohen BL. Nuclear cross sections. In: Brodsky A., ed. Handbook of radiation measurement and protection, Section A: Volume I Physical science and engineering data. West Palm Beach, FL: CRC Press, Inc.; 1978.

Cossairt JD. On residual dose rate within particle accelerator enclosures. Health Phys 71:315-319; 1996.

Cossairt JD. Rule of thumb for estimating groundwater activation from residual dose rates. Batavia, IL: Fermi National Accelerator Laboratory, Environmental Protection Note No. 15; 1998.

Cossairt JD. Radiation physics for personnel and environmental protection. Rev. 9B. Batavia, IL: Fermi National Accelerator Laboratory Report TM-1834; 2007. Available at: http://www-esh.fnal.gov/TM1834_PDF_Files/TM_1834_Revision_9B.pdf. Accessed 22 June 2007.

Fetter CW. Applied hydrogeology. Columbus OH: Merrill Publishing Company; 1988.

Gabriel TA, Santoro RT. Photon dose rates from the interactions of 100 GeV protons in iron and iron-lead beam stops. Part Accel 4:169-186; 1973.

Gollon PJ. Production of radioactivity by particle accelerators. IEEE Trans Nucl Sc. NS 23, No. 4:1395-1400; 1976.

Gollon PJ. Soil activation calculations for the anti-proton target area. Batavia, IL: Fermi National Accelerator Laboratory Report TM-816; 1978.

M. Hoefert. Radiation hazard of induced activity in air as produced by high energy accelerators. In: Proceedings of the second international conference on accelerator radiation dosimetry and experience. Stanford, CA: U. S. Atomic Energy Commission CONF-691101; 1969: 111-120.

Jackson JD, Gilchriese GD, Groom DE, Sanford J, Stevenson GR, Freeman WS, O'Brien K, Thomas RH. SSC environmental radiation shielding. Berkeley, CA: Superconducting Super Collider Central Design Group Report SSC-SR-1026; 1987.

Jackson JD. Classical electrodynamics. 3rd ed. New York, NY: John Wiley and Sons, Inc.; 1999.

Knoll GF. Radiation detection and measurement. 3rd Edition. New York, NY: John Wiley and Sons, Inc.; 2000.

Konobeyev, Korovin A. Tritium production in materials from C to Bi irradiated with nucleons of intermediate and high energies. Nucl Instrum and Meth in Phys Res B82:103-115; 1993.

Konopinski EJ. Electromagnetic fields and relativistic particles. New York, NY: McGraw Hill; 1981.

Malensek AJ, Wehmann AA, Elwyn AJ., Moss KJ, Kesich PM. Groundwater migration of radionuclides at Fermilab. Batavia, IL: Fermi National Accelerator Laboratory Report TM-1851; 1993.

McCaslin JB. A high-energy neutron-flux detector. Health Phys 2:399-407; 1960.

McCaslin JB, Patterson HW, Smith AR, Stephens LD. Some recent developments in technique for monitoring high-energy accelerator radiation. In: Proc. of the First International Congress of Radiation Protection. Belfast, Northern Ireland: International Radiation Protection Association, Pergamon Press; 1968: 1131-1137.

Moritz LE. Measurement of neutron leakage spectra at a 500 MeV proton accelerator. Health Phys 56:287-296; 1989.

Patterson HW, Wallace R. A method of calibrating slow neutron detectors. Berkeley, CA: Lawrence Radiation Laboratory Report UCRL-8359; 1958.

Patterson HW, Thomas RH. Accelerator health physics. New York, NY: Academic Press; 1973.

Rossi B, Griesen K. Cosmic-ray theory. Rev Mod Phys 13:240-309; 1941.

Slade DA, ed. Meterology and atomic energy. Springfield, VA: U. S. Atomic Energy Commission Office of Information Services: TID-24190; 1968.

Stevenson GR. The estimation of dose equivalent from the activation of plastic scintillators. Health Phys 47:837-847; 1984.

Sudicky EA, Wadsworth TD, Kool JB, Huyakorn PS. PATCH 3D; Three dimensional analytical solution for transport in a finite thickness aquifer with first-type rectangular patch source. Waterloo, Ontario, Canada: Prepared for Woodward-Clyde Consultants, Inc. University of Waterloo; 1988.

Sullivan AH, Overton TR. Time variation of the dose-rate from radioactivity induced in high-energy particle accelerators, Health Phys 11:1101-1105;1965.

Swanson WP. Radiological safety aspects of the operation of electron linear accelerators. Vienna, Austria: International Atomic Energy Agency Technical Report No. 188; 1979a.

Swanson WP. Improved calculation of photoneutron yields released by incident electrons. Health Phys 37:347-358; 1979b.

Swanson WP, Thomas RH. Dosimetry for radiological protection at high energy particle accelerators. In: Kase KR, Bjärngard BE, Attix FH, eds. The dosimetry of ionizing radiation, Volume III.. New York, NY**:** Academic Press; 1990: 1-161.

Thomas RH, Stevenson GR. Radiation protection around high energy accelerators. Rad Prot Dos 10:283-301; 1985.

Thomas RH, Stevenson GR. Radiological safety aspects of the operation of proton accelerators. Vienna, Austria: International Atomic Energy Agency Technical Report No. 283; 1988.

Tuli JK. Nuclear wallet cards. 7th ed. Upton, NY: National Nuclear Data Center; Brookhaven National Laboratory; 2005. Available online at www.nndc.bnl.gov. Accessed 25 June 2007.

Tuyn JWN, Deltenre R, Lamberet C, Roubaud. Some radiation aspects of heavy ion acceleration. Geneva, Switzerland: European Organization for Nuclear Research (CERN) Report TIS-RP/125/CF; 1984.

U. S. Code of Federal Regulations. National emissions standard for hazardous air pollutants (NESHAP) for the emission of radionuclides other than radon from Department of Energy facilities. Title 40: Part 61, Subpart H; 1989.

U. S. Code of Federal Regulations. Occupational radiation protection at Department of Energy facilities. Title 10: Part 835; 1998.

U. S. Code of Federal Regulations. National primary drinking water regulations; final rule. Title 40: Parts 141 and 142; 2000.

U. S. Code of Federal Regulations. Occupational radiation protection at Department of Energy facilities. Title 10: Part 835; 2007.

U. S. Department of Energy. Radiation protection of the public and the environment. DOE Order 5400.5; 1990.

Van Ginneken A. Na^{22} production cross section in soil. Batavia, IL. Fermi National Accelerator Laboratory Report TM-283; 1971.

Vaziri K, Cupps V, Boehnlein D, Cossairt D, Elwyn A, Leveling T. AP0 stack monitor calibration. Batavia, IL: Fermi National Accelerator Laboratory Radiation Physics Note No. 106; 1993.

Vaziri K, Cupps VR, Boehnlein D, Cossairt D, Elwyn A. A detailed calibration of a stack monitor used in the measurement of airborne radionuclides at a high energy proton accelerator. Batavia, IL: Fermi National Accelerator Laboratory Report FERMILAB-Pub-96/037; 1994.

Tables

Table 1 Examples of saturation activities and saturation absorbed dose rates at one meter for electrons of energy E_o incident on various target materials of naturally-occurring isotopic abundances normalized to the beam power. [Adapted from Swanson (1979a).]

Target Material	Nuclide	Half-life	Threshold	Specific Gammy Ray Constant Γ		Saturation activity per unit beam power	
			(MeV)	[(mGy h^{-1}) x(GBq m^{-2})$^{-1}$]	[(rad h^{-1}) x (Ci m^{-2})$^{-1}$]	(GBq kW^{-1})	(Ci kW^{-1})
Al	^{24}Na	14.95 h	23.7	0.52	1.9	1.1	0.03
	^{26m}Al	6.34s	13.0	0.17	0.62	330	8.8
Fe	^{54}Mn	312.2 d	20.4	0.34	1.3	22.0	0.29
	^{56}Mn	2.58h	10.6	0.24	0.9	1.12	0.032
	^{53}Fe	8.51 min	13.6	0.19	0.7	27.0	0.74
Ni	^{56}Ni	6.08 d	22.5	0.45	1.7		
	^{56}Co[a]	77.23 d		0.65	2.4	2.4[b]	0.07[b]
	^{57}Ni	35.6 h	12.2	0.38	1.42		
	^{57}Co[a]	217.78 d		0.37	1.36	155[b]	4.2[b]
Cu	^{61}Cu	3.33 h	19.7	0.2	0.75	32.2	0.87
	^{62}Cu	9.67 min	10.8	0.17	0.63	407	11
	^{64}Cu	12.7 h	9.91	0.11	0.40	185	5
W	^{182m}Ta	15.84 min	7.15	0.04	0.16		
	^{182}Ta[a]	114.4 d		0.17	0.64	13.3	0.36
	^{183}Ta	5.1 d	7.71	0.04	0.16	23.3	0.63
	^{181}W	121.2 d	7.99	0.03	0.09	340	9.1
	^{185m}W	1.67 min	7.27	0.05	0.19		
	^{185}W[a]	75.1 d		no γ-ray	no γ-ray	300[b]	8.1[b]
Au	^{195m}Au	30.5 s	14.8	0.04	0.16		
	^{195}Au[a]	186.1 d		0.02	0.07	204[b]	5.5
	^{196m}Au	9.6 h	8.07	0.03	0.12		
	^{196}Au[a]	6.17 d		0.08	0.30	1520[b]	41[b]
Pb	^{203}Pb	6.21 s	8.38	0.05	0.19	17.4	0.47
	^{204m}Pb	1.14 h	14.8	0.32	1.20	44	1.2

[a]This radionuclide is the progeny of the radionuclide above it.
[b]Activity of the progeny radionuclide

Table 2 Estimations of saturation activities and absorbed rates at one meter in various materials, assuming "point source" conditions for high energy electrons. Results have been summed over the naturally-occurring isotopic composition of the materials. Radionuclides contributing <0.1 (mGy h^{-1})(kW m^{-2})$^{-1}$ or with $t_{1/2}$<1 minute have been excluded as have products of thermal neutron capture reactions. [Adapted from Swanson (1979a).]

Material: Natural Aluminum						
Produced Radionuclide			Saturation Activity per Unit Beam Power		Saturation Absorbed Dose per Unit Beam Power[a]	
	Half-life	Threshold (MeV)	(GBq kW^{-1})	(Ci kW^{-1})	(mGy h^{-1})x (kW m^{-2})$^{-1}$	(rad h^{-1})x (kW m^{-2})$^{-1}$
^{7}Be	53.22 d	33.0	4.8	0.13	0.04	0.004
^{11}C	20.33 min	33.5	1.9	0.051	0.3	0.03
^{15}O	2.04 min	33.4	2.5	0.07	0.4	0.04
^{18}F	1.83 h	34.4	5.2	0.14	0.8	0.08
^{22}Na	2.60 y	22.5	9.2	0.25	3.0	0.3
^{24}Na	14.95 h	23.7	10.4	0.28	5.0	0.5
^{26m}Al	6.34 s	13.0	320	8.8	60.0	6.0
Material: Natural Iron						
^{46}Sc	83.79 d	37.4	7.4	0.2	2.0	0.2
^{48}V	15.97 d	25.9	15.0	0.4	8.0	0.8
^{51}Cr	27.70 d	19.7	15.0	0.4	3.0	0.3
^{52}Mn	5.59 h	20.9	1.5	0.04	0.4	0.04
^{52m}Mn	21.1 min	20.9	1.5	0.04	0.4	0.04
^{54}Mn	312.1 d	20.4	22.0	0.59	7.0	0.7
^{56}Mn	2.58 h	10.6	1.1	0.03	0.3	0.03
^{52}Fe	8.28 h	24.1	2.2	0.06	0.4	0.04
^{53}Fe	8.51 min	13.6	27.4	0.74	4.9	0.49
^{55}Fe	2.74 y	11.2	490	13.3	90	9
Material: Natural Copper						
^{58m}Co	9.04 h	41.8	24.4	0.66	4.0	0.4
^{58}Co	70.9 d	41.8	240=.4	0.66	2.0	0.2
^{60}Co	5.27 y	18.9	24.0	0.65	8.0	0.8
^{63}Ni	100 y	17.1	16.6	0.45	no γ-rays	no γ-rays
^{61}Cu	3.33 h	19.7	32.2	0.87	6.0	0.6
^{62}Cu	9.64 min	10.8	407	11	65	6.5
^{64}Cu	12.7 h	9.9	180	5	19	1.9

[a]"no γ-rays" is applied to radionuclides having no, or very rare, emissions of photons in their decay.

Table 2-continued

Produced Radionuclide			Saturation Activity per Unit Beam Power		Saturation Absorbed Dose per Unit Beam Power[a]	
	Half-life	Threshold (MeV)	(GBq kW^{-1})	(Ci kW^{-1})	(mGy h^{-1})x (kW m^{-2})$^{-1}$	(rad h^{-1})x (kW m^{-2})$^{-1}$
Material: Natural Tungsten						
^{182m}Ta	15.84 min	7.15	13.3	0.36	0.3	0.03
^{182}Ta	114.4 d	7.15	13.3	0.36	1.1	0.11
^{183}Ta	5.1d	7371	22.9	0.62	0.9	0.09
^{184}Ta	8.7 h	14.9	1.78	0.048	0.4	0.04
^{185}Ta	49.4 min	8.39	20.7	0.56	0.6	0.06
^{181}W	121.2 d	8.00	330	8.9	8.0	0.8
^{185m}W	1.67 min	7.27	300	8.1	7.3	0.73
^{185}W	75.1 d	7.27	300	8.1	no γ-rays	no γ-rays
Material: Natural Lead						
^{204}Tl	3.78 y	14.83	0.92	0.025	no γ-rays	no γ-rays
^{206}Tl	4.20 min	7.46	37	1.0	no γ-rays	no γ-rays
^{207m}Tl	1.33 s	8.04	93	2.5	9.1	0.91
^{207}Tl	4.77 min	8.04	93	2.5	no γ-rays	no γ-rays
^{202m}Pb	3.53 h	15.3	0.13	0.06	0.3	0.03
^{202}Pb	5.25×10^4 y	15.3	0.13	0.06	no γ-rays	no γ-rays
^{203m}Pb	6.21 s	8.38	31	0.83	1.3	0.13
^{203}Pb	2.16 d	8.38	31	0.83	0.7	0.07
^{204m}Pb	1.14 h	14.8	89	2.4	14	1.4
Material: Typical Concrete[b]						
^{15}O	2.04 min	15.7	96	2.6	15	1.5
^{22}Na	2.60 y	12.4	3.7	0.1	1.2	0.12
^{27}Si	4.16	17.2	74	2.0	12	1.2
^{38}K	7.64 min	13.1	3.7	0.1	15	0.15

[a]"no γ-rays" is applied to radionuclides having no, or very rare, emission of photons in their decay.

[b]By weight per cent, the isotopic composition of concrete was taken to be: ^{12}C (0.10), ^{16}O (53.0), ^{23}Na (1.6), ^{24}Mg (0.16), ^{27}Al (3.4), ^{28}Si (31.0), ^{39}K (1.2), ^{54}Fe (0.08), all others (9.5).

Table 3 Tabulation of generalized parameters for the production of radionuclides by means of low energy nuclear reactions. The ranges of energies are listed at which the production yields are at approximately 0.1 per cent of the tabulated saturation values. The "high/low" values for the saturated activity are also given. [Adapted from Cohen (1978).]

Reaction	0.1% Yield-low (E-E_{th}) (MeV)	0.1% Yield-high (E-E_{th}) (MeV)	Saturation Yield-Low		Saturation Yield-High	
			(MBq/μA)	(μCi/μA)	(MBq/μA)	(μCi/μA)
(p,γ)	4	9	11	3×10^2	37	10^3
(p,n)	0	6	1.1×10^4	3×10^5	3.0×10^4	8×10^5
(p,2n)	1	4	1.1×10^4	3×10^5	3.7×10^4	10^6
(p,3n)	1	6	1.1×10^4	3×10^5	3.7×10^4	10^6
(p,4n)	5	8	7.4×10^3	2×10^5	3.7×10^4	10^6
(p,5n)	5	10	3.7×10^3	10^5	7.4×10^4	2×10^6
(p,pn)	2	5	7.4×10^3	2×10^5	7.4×10^4	2×10^6
(p,p2n)	3	8	1.1×10^4	3×10^5	7.4×10^4	2×10^6
(d,γ)	5	7	1.1	30	3.7	1×10^2
(d,n)	2	7	1.5×10^2	4×10^3	1.1×10^4	3×10^5
(d,2n)	2	5	7.4×10^3	2×10^5	2.2×10^5	6×10^6
(d,3n)	1	4	1.1×10^4	3×10^5	3.7×10^4	10^6
(d,4n)	4	8	7.4×10^3	2×10^5	2.2×10^4	6×10^5
(d,5n)	6	10	3.7×10^3	10^5	3.7×10^4	10^6
(d,p)	2	7	1.5×10^3	4×10^4	1.1×10^4	3×10^5
(d,p2n)	2	10	3.7×10^3	10^5	7.4×10^4	2×10^6
(d,p3n)	8	15	3.7×10^3	10^5	7.4×10^4	2×10^6
(d,2p)	5	15	1.1×10^2	3×10^3	1.5×10^3	4×10^4
(d,α)	4	7	3.7×10^2	10^4	1.1×10^3	3×10^4
(d,αn)	5	15	7.4×10^2	2×10^4	3.7×10^3	10^5
(^{3}He,γ)	4	6	3.7×10^{-2}	1	7.4×10^{-2}	2
(^{3}He,n)	3	12	3.7	10^2	11	3×10^2
(^{3}He,2n)	2	7	11	3×10^2	1.5×10^2	4×10^3
(^{3}He,3n)	2	5	74	2×10^3	1.1×10^3	3×10^4
(^{3}He,2p)	4	12	7.4	2×10^2	3.7×10^2	10^4
(^{3}He,α)	6	14	7.4	2×10^2	37	10^3
(^{3}He,p3n)	10	15	3.7×10^2	10^4	1.5×10^4	4×10^5
(α,γ)	10	13	0.11	3	0.74	20
(α,n)	1	9	11	3×10^2	3.7×10^2	10^4
(α,2n)	1	4	1.8×10^2	5×10^3	1.5×10^3	4×10^4
(α,3n)	1	6	1.1×10^2	3×10^3	1.6×10^4	7×10^5
(α,4n)	5	8	1.1×10^2	3×10^3	1.5×10^3	4×10^4
(α,5n)	5	8	3.7×10^2	10^4	1.1×10^4	3×10^5
(α,p)	5	8	22	6×10^2	7.4×10^2	2×10^4
(α,pn)	3	12	1.1×10^2	3×10^3	3.0×10^3	8×10^4
(α,p2n)	5	15	1.1×10^2	3×10^3	2.6×10^3	7×10^4
(α,p3n)	7	15	3.7×10^2	10^4	1.1×10^3	3×10^4
(α,2p)	5	10	3.7	10^2	1.1×10^2	3×10^3
(α,αn)	6	16	1.1×10^2	3×10^3	1.1×10^3	3×10^4

Table 4 Summary of radionuclides commonly identified in materials irradiated around accelerators. Approximate cross sections for their production at the high energy limit and approximate thresholds are given for selected radionuclides. [Adapted from Barbier (1969).]

Target Material	Radionuclides	Approximate Threshold (MeV)	Half-life	Production Cross Section (High Energy Limit) (mb)
Plastics & Oils	^{3}H	11	12.33 y	10
	^{7}Be	2	53.22 d	10
	^{11}C	20	20.33 min	20
Al, Concrete	As above, plus			
	^{18}F	40	1.83 h	6
	^{22}Na	30	2.60 y	10
	^{24}Na	5	14.95 h	10
Fe	As above, plus			
	^{42}K		12.32 h	
	^{43}K		22.3 h	
	^{44}Sc		3.97 h	
	^{44m}Sc		2.44 d	
	^{46}Sc		83.8 d	
	^{47}Sc		3.35 d	
	^{48}Sc		1.82 d	
	^{48}V	20	15.97 d	6
	^{51}Cr	30	27.7 d	30
	^{52}Mn	20	5.59 d	30
	^{52m}Mn		21.1 min	
	^{54}Mn	30	312.1 d	30
	^{52}Fe	30	8.28 h	4
	^{55}Fe		2.74 y	
	^{59}Fe		44.5 d	
	^{56}Co	5	77.2 d	30
	^{57}Co	30	271.7 d	30
	^{58}Co	30	70.9 d	25
Cu	As above, plus			
	^{57}Ni	40	35.6 h	2
	^{65}Ni		2.52 h	
	^{60}Co	30	5.27 y	15
	^{60}Cu		23.7 min	
	^{61}Cu	20	3.33 h	100
	^{62}Cu		9.67 min	
	^{64}Cu		12.70 h	
	^{62}Zn	15	9.19 h	60
	^{65}Zn	0	243.7 d	100

Table 5 Abundances of the most prominent stable nuclides in the atmosphere at sea level.

Nuclide	Percentage by volume in the atmosphere (atoms)	N_j at room temperature (atoms cm^{-3})
^{14}N	78.16	4.199×10^{19}
^{16}O	20.00	1.075×10^{19}
^{40}Ar	0.467	1.558×10^{17}
^{15}N	0.290	2.149×10^{16}
^{18}O	0.040	1.255×10^{17}

Table 6 Radionuclides with half-life greater than 1 minute that can be produced in air at accelerators. [Adapted from Swanson and Thomas (1990).]

Radionuclide	Half-life	Emission	Parent Element	Production Mechanism	High Energy Cross Section (mb)
^{3}H	12.32 y	β^-	N	Spallation	30
			O	Spallation	30
^{7}Be	53.22 d	γ, elect. capt.	N	Spallation	10
			O	Spallation	5
			Ar	Spallation	0.6
^{11}C	20.33 min	β^+	N	Spallation	10
			O	Spallation	0.7
			Ar	Spallation	0.7
^{14}C	5700 y	β^-	N	$(n_{thermal},p)$	1640
^{13}N	9.96 min	β^+	N	Spallation	10
			N	(γ,n)	10
			O	Spallation	9
			Ar	Spallation	0.8
^{14}O	1.18 min	β^+,γ	O	Spallation	1
			Ar	Spallation	0.06
^{15}O	2.04 min	β^+	O	Spallation	40
			O	(γ,n)	10
			Ar	Spallation	
^{18}F	1.83 h	β^+,	Ar	Spallation	6
^{24}Ne	3.38 min	β^-,γ	Ar	Spallation	0.12
^{22}Na	2.603 y	β^+,γ	Ar	Spallation	10
^{24}Na	14.95 h	β^-	Ar	Spallation	7
^{27}Mg	9.46 min	β^-,γ	Ar	Spallation	2.5
^{28}Mg	20.92 h	β^-,γ	Ar	Spallation	0.4
^{28}Al	2.24 min	β^-,γ	Ar	Spallation	13
^{29}Al	6.56 min	β^-,γ	Ar	Spallation	4
^{31}Si	2.62 h	β^-,γ	Ar	Spallation	6
^{30}P	2.50 min	β^+,γ	Ar	Spallation	4.4
^{32}P	14.26 d	β^-	Ar	Spallation	25
^{33}P	25.34 d	β^-	Ar	Spallation	9
^{35}S	87.51 d	β^-	Ar	Spallation	23
^{34m}Cl	32.0 min	β^-,γ	Ar	Spallation	0.7
^{38}Cl	37.24 min	β^-,γ	Ar	(γ,pn)	4
^{39}Cl	55.6 min	β^-,γ	Ar	(γ,p)	7
^{41}Ar	1.83 h	β^-,γ	Ar	$(n_{thermal},\gamma)$	660

Table 7 Relation of turbulence types to weather conditions. [Adapted from Slade (1968).]

A-Extremely unstable conditions	D-neutral conditions[a]
B-Moderately unstable conditions	E-Slightly stable conditions
C-Slightly unstable conditions	F-Moderately stable conditions

Surface Wind Speed (m/sec)	Daytime insolation			Nightime conditions	
	Strong	Moderate	Slight	Thin overcast or ≥ 4/8 cloudiness[b]	≤ 3/8 cloudiness
<2	A	A-B	B		
2	A-B	B	C	E	F
4	B	B-C	C	D	E
6	C	C-D	D	D	D
>6	C	D	D	D	D

[a]Applicable to heavy overcast, day or night

[b]The degree of cloudiness is defined as that fraction of the sky above the local apparent horizon which is covered by clouds.

Table 8 Derived Air Concentrations (DACs) and Derived Concentration Guides (airborne exposure pathway) for radiation workers and the general population. These represent maximum concentrations $C_{max,i}$ for use in Eq. (51) for individual radionuclides, depending upon the circumstances of exposure[a]. In general, where ambiguities exist, the most conservative value is listed.

	DAC- U. S. DOE Radiation Worker						DCG-General Population[d]	
	Inhaled Air Exposure[b] [50 mSv y^{-1} (40 h $week^{-1}$)]		Immersion Exposure [50 mSv y^{-1} (40 h $week^{-1}$)]				[1 mSv $year^{-1}$ (168 h $week^{-1}$)]	
			Infinite Radius Cloud[b]		4 m Radius Cloud[c]			
	(μCi m^{-3})	(Bq m^{-3})	(μCi m^{-3})	(Bq m^{-3})	(μCi m^{-3})	(Bq m^{-3})	(μCi m^{-3})	(Bq m^{-3})
^{3}H	20	8×10^{5}	unlisted	unlisted	unlisted	unlisted	0.1	3.7×10^{3}
^{7}Be	8	3×10^{5}	unlisted	unlisted	unlisted	unlisted	0.04	1.5×10^{3}
^{11}C	200	6×10^{6}	4	1×10^{5}	59	2.2×10^{6}	0.02	7.4×10^{2}
^{13}N	unlisted	unlisted	4	1×10^{5}	41	1.5×10^{6}	0.02	7.4×10^{2}
^{15}O	unlisted	unlisted	4	1×10^{5}	27	1.0×10^{6}	0.02	7.4×10^{2}
^{22}Na	0.3	1×10^{4}	unlisted	unlisted	unlisted	unlisted	0.001	37
^{24}Na	2	8×10^{4}	0.9	3×10^{4}	unlisted	unlisted	0.004	1.5×10^{2}
^{41}Ar	unlisted	unlisted	3	1×10^{5}	47	1.8×10^{6}	0.01	3.7×10^{2}

[a]Given the primacy of "customary" rather than SI units in United States Regulations, the former is generally taken to be limiting quantity. Furthermore, conversion between the two sets of units in regulatory tables is generally only performed to one significant figure, as reflected here. Where choices needed to be made between day, week, or year exposures, the most restrictive value was taken.

[b](U. S. Code of Federal Regulations 1998) Note: These entries do not reflect modifications that will be necessary under promulgated revisions to the regulations (U. S. Code of Federal Regulations 2007).

[c](Hoefert 1969) These values are not to be used for regulatory compliance purposes.

[d](U. S. Department of Energy 1990) The values listed are the most restrictive given in two different tables. This results given in Bq m^{-3} were calculated from the μCi m^{-3} entries.

Table 9 Estimated saturation activities per unit bremsstrahlung path length and per unit beam power produced in air by an electron beam normalized to the beam power. "Cross section" ($\Sigma f\sigma$) refers to the integral radionuclide production cross section per MeV of beam energy inclusive of the natural isotopic abundance in air (see Table 5). [Adapted from Swanson (1979a).]

Produced Radionuclide		Parent Stable Nuclide			Cross Section, $\Sigma f\sigma$	Saturation Activity per Unit Length and Beam Power[a]	
Nuclide	Half-life	Nuclide	Reaction Type	Threshold (MeV)	($\mu b\ MeV^{-1}$)	($MBq\ m^{-1}\ kW^{-1}$)	($\mu Ci\ m^{-1}\ kW^{-1}$)
^{3}H	12.32 y	^{14}N	$(\gamma,^{3}H)$	22.7	3		
		^{16}O	$(\gamma,^{3}H)$	25.0	3	5.2	140
^{7}Be	53.22	^{14}N	$(\gamma,sp)^{b}$	37.8	0.6		
		^{16}O	$(\gamma,sp)^{b}$	31.9	0.6	1.11	30
^{11}C	20.33 min	^{12}C	(γ,n)	18.7	0.011		
		^{14}N	$(\gamma,sp)^{b}$	22.7	6		
		^{16}O	$(\gamma,sp)^{b}$	25.9	6	11	300
^{13}N	9.96 min	^{14}N	(γ,n)	10.6	310	520	1.4×10^{4}
^{15}O	2.04 min	^{16}O	(γ,n)	15.7	32	55.5	1.5×10^{3}
^{16}N	7.13 s	^{18}O	(γ,np)	21.8	0.01	0.018	0.5
^{38}Cl	37.24 min	^{40}Ar	(γ,np)	20.6	0.13	0.22	6
^{39}Cl	55.6 min	^{40}Ar	(γ,p)	12.5	0.86	1.5	40
^{41}Ar	1.83 h	^{40}Ar	$(n,\gamma)^{c}$	-	-	variable	variable

[a]Normalized per bremsstrahlung pathlength in air (m) and electron beam power (kW) incident on a high-Z target, summed over individual contributing reactions.
[b]Spallation reaction
[c]Thermal neutron capture reaction that where high neutron fluences are moderated by water or concrete shielding.

Table 10 Measured examples of radionuclide compositions of typical airborne releases at proton accelerators.

Situation	Radionuclides (Activity Per Cent)					
	^{11}C	^{13}N	^{15}O	^{38}Cl	^{39}Cl	^{41}Ar
CERN 28 GeV protons[a]	31.0	47.0	8.0			14.0
Fermilab 800 GeV protons[b]						
no gap between iron and concrete walls	46.0	19.0	35.0			
gap between iron and concrete walls	42.0	14.0	0.0	0.0	10.0	34.0
Fermilab 120 GeV protons[c]	58.5	37.9		1.0	1.1	1.5
Fermilab 120 GeV protons[d]	64.6	30.5				5.0

[a](Thomas and Stevenson 1988)
[b](Butala et al. 1989)
[c](Vaziri et al. 1993)
[d](Vaziri et al. 1996)

Table 11 Estimated saturation activities in water per unit beam power produced in ^{16}O by an electron beam normalized to the beam power. [Adapted from Swanson (1979a).]

Produced Radionuclide		Reaction Parameters			Specific Gammy Ray Constant, Γ		Saturation Activity per Unit Beam Power	
	Half-life	Reaction	Threshold (MeV)	Cross Section, σ ($\mu b\ MeV^{-1}$)	(mGy h^{-1}) x(GBq m^{-2})$^{-1}$	(rad h^{-1}) x (Ci m^{-2})$^{-1}$	(GBq kW^{-1})	(Ci kW^{-1})
^{3}H[a]	12.32 y	(γ,^{3}H)	25.0	1.5	-	-	7.4	0.2
^{7}Be	53.22 d	(γ,5n4p)	31.9	0.3	0.008	0.03	1.5	0.04
^{10}C	19.26 s	(γ,4n2p)	38.1	1	0.29	1.06	3.7	0.1
^{11}C	20.33 min	(γ,3n2p)	25.9	3	0.17	0.62	14.8	0.4
^{13}N	9.96 min	(γ,2np)	25.0	0.9	0.17	0.62	3.7	0.1
^{14}O	1.18 min	(γ,2n)	28.9	1	0.45	1.7	3.7	0.1
^{15}O	2.04 min	(γ,n)	15.7	75	0.17	0.62	330	9

[a]Does not present an external radiation hazard.

Table 12 Composition of soils typical of the Fermilab site. [Adapted from Borak et al. (1972).]

Elemental Composition of Soil[a]		
Element	*Z*, Atomic Number	% by Weight
Silicon	14	14.47
Aluminum	13	2.44
Iron	26	1.11
Calcium	20	7
Magnesium	12	3.79
Carbon	6	5.12
Sodium	11	0.34
Potassium	19	0.814
Oxygen	8	≈ 64

[a]The mean moisture percentage was 13.15±4.45 % and the mean pH was 7.6±0.1.

Table 13 Macroscopic cross section for soil normalized to unit flux of hadrons with kinetic energies greater than 30 MeV. [Adapted from Borak et al. (1972).]

Nuclide	Glacial Till Σ (cm^2 g^{-1})	Gray Sandy Clay Σ (cm^2 g^{-1})	Red Sandy Clay Σ (cm^2 g^{-1})	Gray Clay Σ (cm^2 g^{-1})
^{7}Be	2.9×10^{-4}	3.7×10^{-4}	3.2×10^{-4}	2.7×10^{-4}
^{51}Cr	1.7×10^{-5}	3.7×10^{-5}	2.8×10^{-5}	3.1×10^{-5}
^{22}Na	2.1×10^{-4}	2.3×10^{-4}	2.0×10^{-4}	1.6×10^{-4}
^{54}Mn	5.9×10^{-5}	4.1×10^{-5}	3.5×10^{-5}	3.7×10^{-5}
^{46}Sc	3.0×10^{-5}	1.3×10^{-5}	9.6×10^{-6}	1.1×10^{-5}
^{48}V	4.1×10^{-6}	1.1×10^{-5}	6.7×10^{-6}	7.4×10^{-6}
^{55}Fe	9.3×10^{-5}	1.2×10^{-4}	7.0×10^{-5}	2.1×10^{-4}
^{59}Fe	3.2×10^{-6}	1.7×10^{-6}	1.3×10^{-6}	1.6×10^{-6}
^{60}Co	3.3×10^{-5}	1.4×10^{-5}	1.1×10^{-5}	1.3×10^{-5}
^{45}Ca	1.6×10^{-4}	2.0×10^{-5}	3.0×10^{-5}	1.6×10^{-5}
^{3}H	8.2×10^{-4}	1.1×10^{-3}	3.3×10^{-4}	5.2×10^{-4}
$^{3}H^{a}$	5.9×10^{-3}	5.9×10^{-3}	4.1×10^{-3}	4.4×10^{-3}

[a]Cross sections per gram of water in soil.

Table 14 Examples of typical values of hydraulic conductivity. [Adapted from Batu (1998).]

Group	Porous Materials	Range of K values (cm s^{-1})
Igneous Rocks	Weathered granite	(3.3-52) x 10^{-4}
	Weathered gabbro	(0.5-3.8) x 10^{-4}
	Basalt	(0.2-4250) x 10^{-6}
Sedimentary Materials	Sandstone (fine)	(0.5-2250) x 10^{-6}
	Siltstone	(0.1-142) x 10^{-8}
	Sand (fine)	(0.2-189) x 10^{-4}
	Sand (medium)	(0.9-567) x 10^{-4}
	Sand (coarse)	(0.9-6610) x 10^{-4}
	Limestone and dolomite	(0.4-2000) x 10^{-7}
	Karst limestone	(1-20000) x 10^{-4}
	Gravel	(0.3-31.2) x 10^{-1}
	Silt	(0.09-7090) x 10^{-7}
	Clay	0.1-47) x 10^{-8}
Metamorphic Rocks	Schist	(0.002-1130) x 10^{-6}

Table 15 Important characteristics of various nuclear reactions used in activation detectors.

Detector	Reaction	Energy Range (MeV)	Half-Life	Typical Detector Size	Cross Section-Peak (mb)	Cross Section-High Energy(mb)	Particle Detected
sulfur	$^{32}S(n,p)^{32}P$	> 3	14.26 d	4 g disk	500[a]	10[a]	β^-
aluminum	$^{27}Al(n,\alpha)^{24}Na$	> 6	14.95 h	16 - 6600 g	11[b]	9[b]	γ
aluminum	$^{27}Al(n,x)^{22}Na$	> 25	2.603 y	17 g	30[b]	10[b]	γ
plastic scintillator	^{12}C-> ^{11}C	> 20	20.33 min	13-2700 g	90[b]	30[b]	β^+, γ
plastic scintillator	^{12}C->^{7}Be	> 30	53.22 d	17 g	18[b]	10[b]	γ
mercury	^{198}Hg->^{149}Tb	> 600	4.12 h	up to 500 g	2[b]	1[b]	α,γ
gold	^{197}Au->^{149}Tb	> 600	4.12 h	0.5 g	1.6[b]	0.7[b]	α,γ
copper	Cu->^{24}Na	> 600	14.95 h	580 g	4[c]	3.9[c]	γ
copper	Cu->^{52}Mn	> 70	5.59 d	580 g	5[c]	4.6[c]	γ
copper	Cu->^{54}Mn	> 80	312.1 d	580 g	11[c]	11[c]	γ

[a]Swanson and Thomas (1990)
[b]Barbier (1969)
[c]Baker et al. (1984) and Baker et al. (1991).

Figure Captions

1. Examples of excitation functions for important photon-induced reactions (upper frame) and for the special case of photo-pion reactions (lower frame) at intermediate energies. [Adapted from Barbier (1969).]
2. Neutron yields from infinitely thick targets per kW of electron beam power as a function of electron beam energy E_O, ignoring target self-shielding. [Adapted from Swanson (1979b).]
3. Examples of total photon absorbed dose rates due to radioactive nuclei produced in large targets of various materials irradiated by an electron current of one electron sec^{-1} per MeV incident electron energy as a function of time since the cessation of the irradiation. The irradiation was assumed to have occurred for an infinitely long period of time. The absorbed dose rates are those found at one meter from a point source containing all of the radioactive nuclei. [Adapted from Barbier (1969).]
4. Examples of excitation functions for the production of various radionuclides by protons incident on some light targets. In the lower frame, "?" in the statement of the nuclear reaction implies inclusion of all possible outgoing particles that could be emitted. [Adapted from Barbier (1969).]
5. Excitation functions for the production of various radionuclides by protons incident on iron and copper targets. [Adapted from Barbier (1969).]
6. Typical behavior of radionuclide production by (p,γ) or few-nucleon transfer reactions for energies not far above the reaction threshold E_{th}. This behavior is typical of the nuclear reactions tabulated in Table 3. For detailed calculations, data related to specific reactions on specific target materials should be used. [Adapted from Cohen (1978).]

7. Total number of radionuclides having half-lives up to a given half-life as a function of half-life for target mass numbers less than those indicated. [Adapted from Barbier (1969).]

8. Values of the Barbier danger parameter **D** for aluminum, iron and copper at a proton irradiation energy of 500 MeV. [Adapted from Barbier (1969).]

9. Values of the Barbier danger parameter **D** for tungsten and $CaCO_3$ at a proton irradiation energy of 500 MeV. [Adapted from Barbier (1969).]

10. Cooling curves for various irradiation times for iron struck by high energy protons as calculated by Armstrong and Alsmiller (1969). Also shown are the results of measurements. The one labeled "Main Ring", is the measured average cooling curve for the Fermilab Main Ring synchrotron after its initial three years of operation at energies of 200 or 400 GeV. The curve labeled "Neutrino" is for a target station used to produce high energy neutrinos copiously at Fermilab after eight months of operation at 400 GeV with high intensity proton beams. The curve labeled "AGS" is for an extraction splitter in use for many years at the BNL AGS at energies up to 30 GeV. [Adapted from Gollon (1976).]

11. Extrapolations of the cooling factor $\omega(t_i, t_c)$ from the work of Armstrong and Alsmiller (Ar69) and Gabriel and Santoro (Ga73) compared with those of Gollon (Go76) for irradiated iron. [Adapted from Cossairt (1998).]

12. Geometry for deriving the relationship between a surface of uniform emission and the flux density at any point within it. [Adapted from Cossairt (1996).]

13. Photon dose rate at surface of tunnel wall after infinite irradiation time for concrete containing one per cent sodium by weight. [Adapted from Armstrong and Barish (1969).]

14. Horizontal diffusion constants σ_y as a function of downwind distance *x* from the source for turbulence types defined in Table 7. [Adapted from Slade (1968).]

15. Vertical diffusion constants σ_z as a function of downwind distance *x* from the source for turbulence types defined in Table 8.5. [Adapted from Slade (1968).]

16. Cross sections for the production of ^{3}H due to neutron bombardment of materials commonly found in soil and rock as a function of neutron energy calculated following the method of Konobeyev and Korovin (1993). Results for aluminum are similar to those found for silicon and those for sodium are similar to those found for magnesium.

17. Cross sections for the production of ^{22}Na due to neutron bombardment of materials commonly found in soil and rock as a function of neutron energy. Results for potassium are quite similar to those found for calcium. [Adapted from Van Ginneken (1971).]

18. Hydrogeological model of a shallow well in proximity to an accelerator tunnel where a beam loss occurs. The radioactivated region is represented in cross section by the cross-hatched rectangle to the right. *h* represents the elevation of the water table above the impervious stratum as a function of *r* while the water table is a distance *H* above the impervious stratum where the water table is not perturbed by wells. [Adapted from Jackson et al. (1987).]

19. Excitation functions for the reactions $^{12}C->^{11}C$ induced by neutrons, pions, and protons. The arithmetic mean of the positive and negative pions cross sections is shown as the pion curve. [Adapted from Swanson and Thomas (1990).]

20. Excitation functions of several threshold reactions. [Adapted from Thomas and Stevenson (1988).]

21 Fission cross sections of some common target nuclides used in fission chambers for fast

neutrons. The cross sections for fission of ^{235}U are much larger at lower energies not shown. [Adapted from Knoll (1979) and Swanson and Thomas (1990).]

Fig. 1

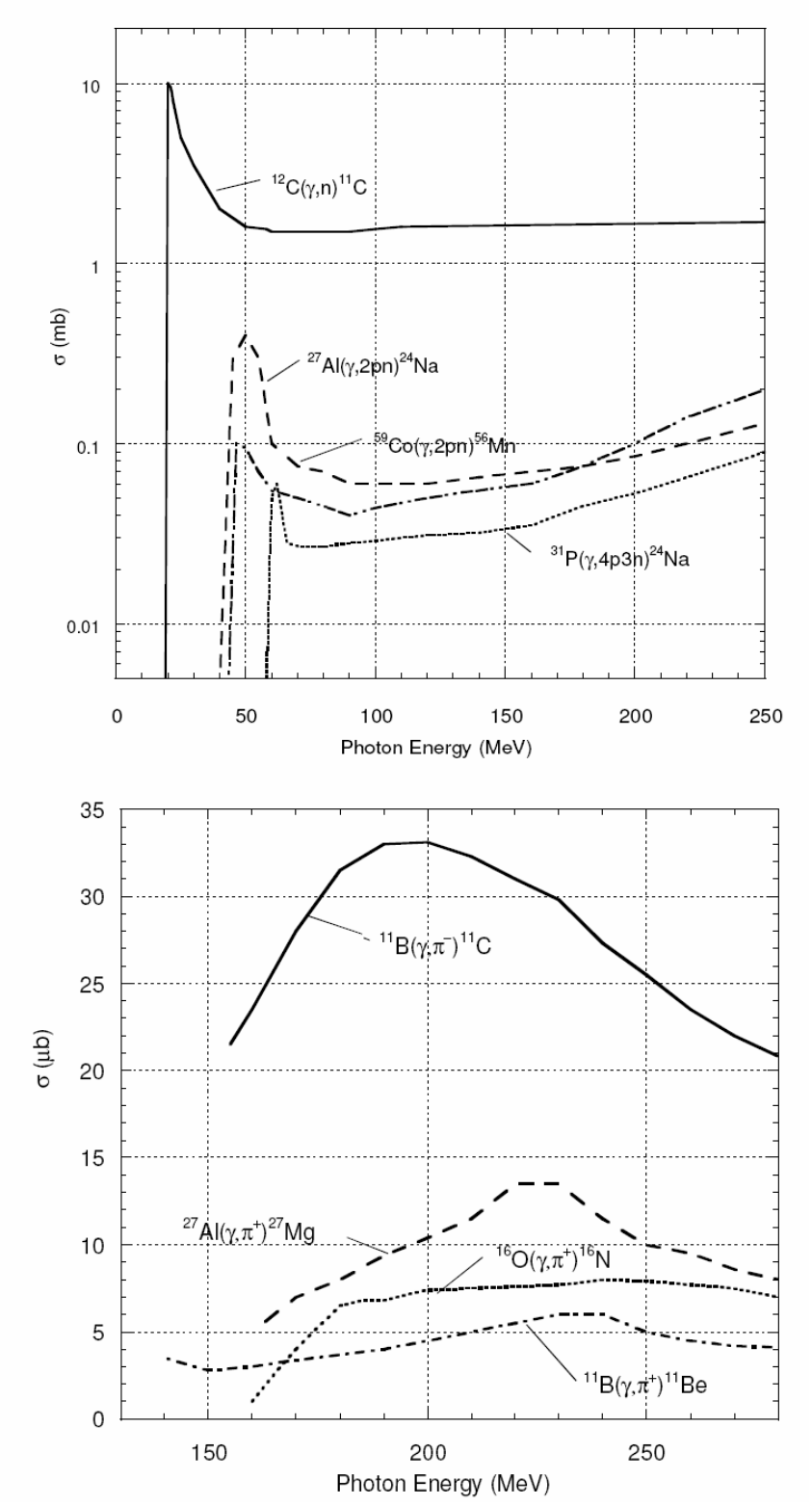
10
1
0.1
0.01
σ (mb)
$^{12}C(\gamma,n)^{11}C$
$^{27}Al(\gamma,2pn)^{24}Na$
$^{59}Co(\gamma,2pn)^{56}Mn$
$^{31}P(\gamma,4p3n)^{24}Na$
0
50
100
150
200
250
Photon Energy (MeV)
35
30
25
20
15
10
5
0
σ (μb)
$^{11}B(\gamma,\pi^-)^{11}C$
$^{27}Al(\gamma,\pi^+)^{27}Mg$
$^{16}O(\gamma,\pi^+)^{16}N$
$^{11}B(\gamma,\pi^+)^{11}Be$
150
200
250
Photon Energy (MeV)

Fig. 2

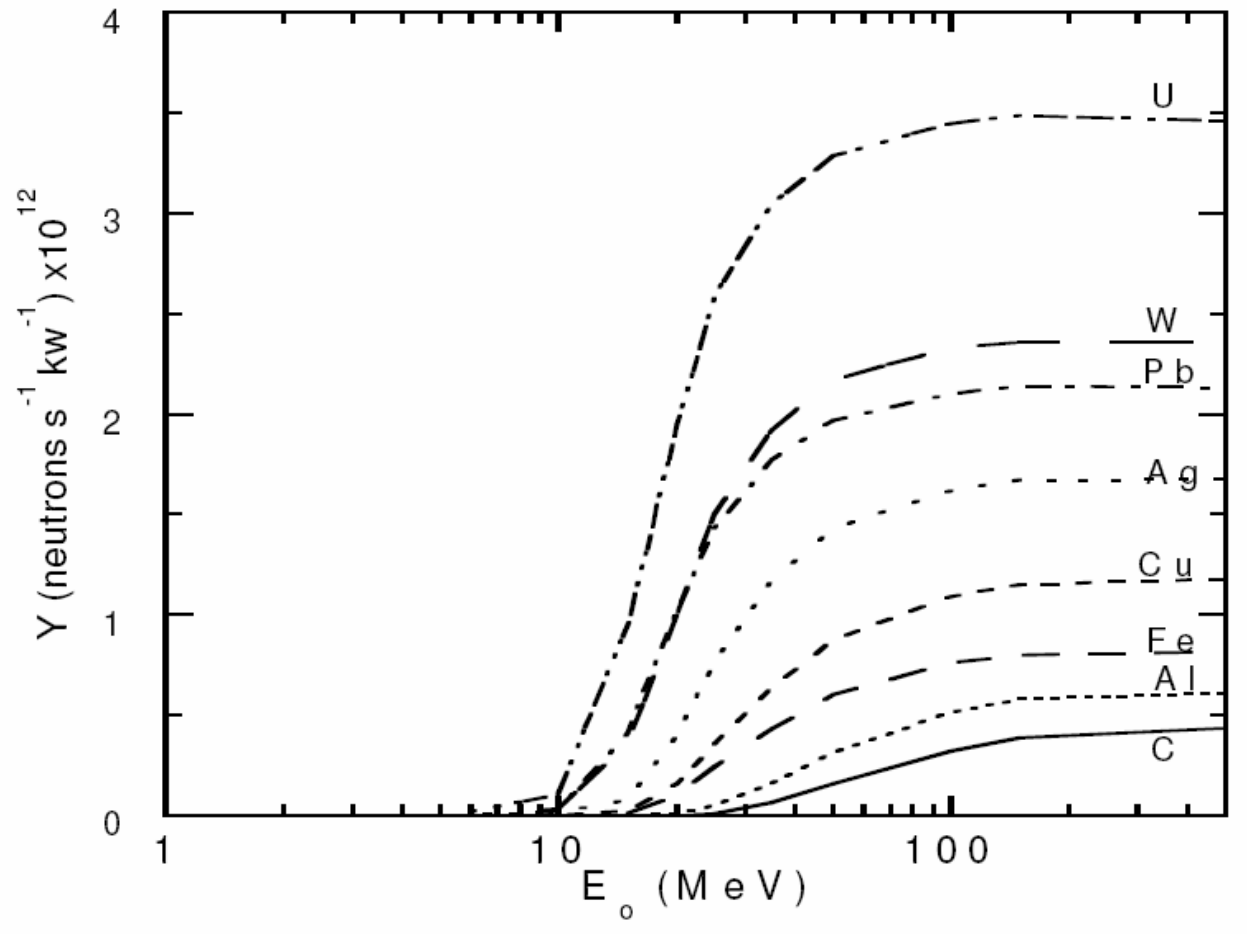

Fig. 3

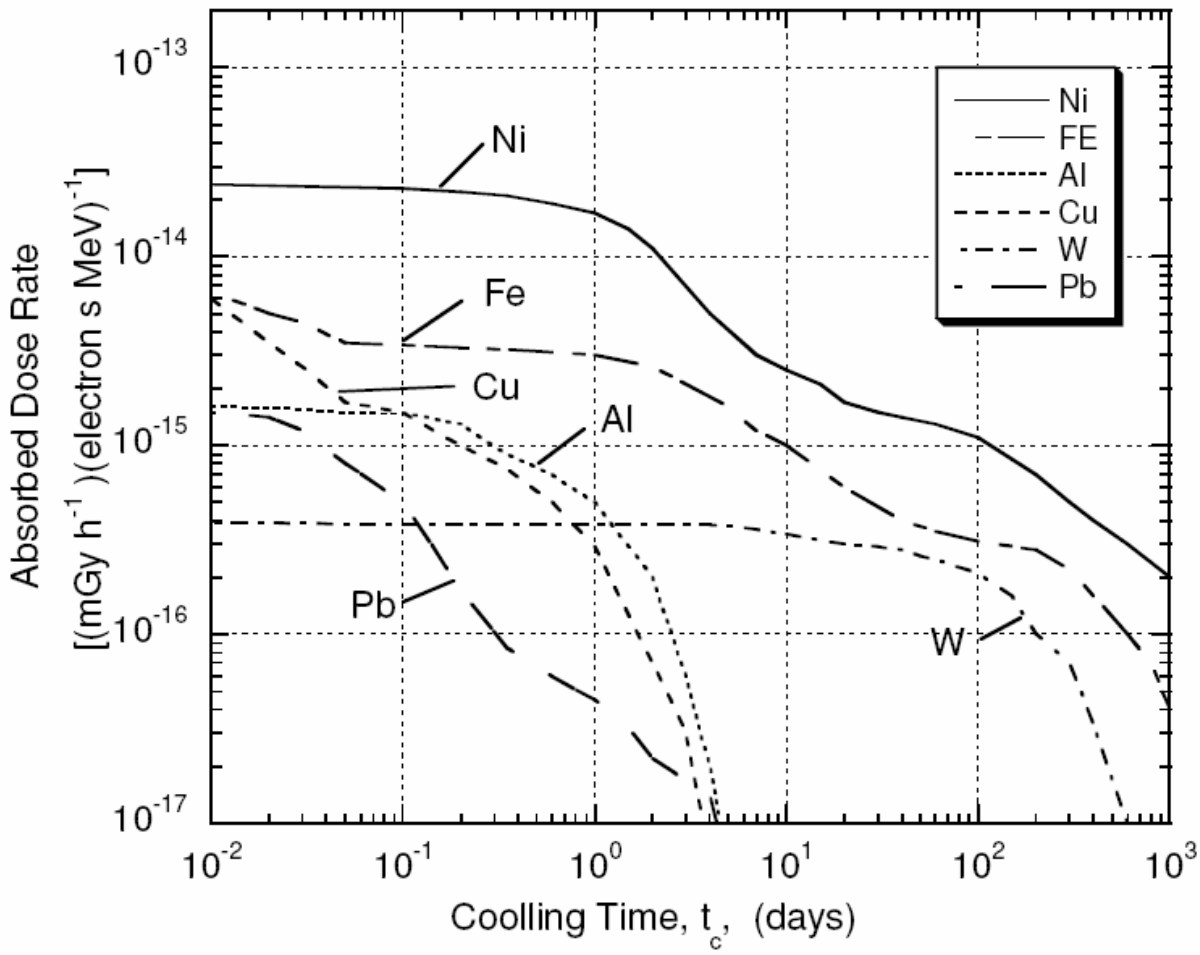
Absorbed Dose Rate
[(mGy h-1)(electron s MeV)-1]
Coolling Time, tc, (days)
Ni
Fe
Cu
Al
Pb
W
Ni
FE
Al
Cu
W
Pb
10-13
10-14
10-15
10-16
10-17
10-2
10-1
100
101
102
103

Fig. 4

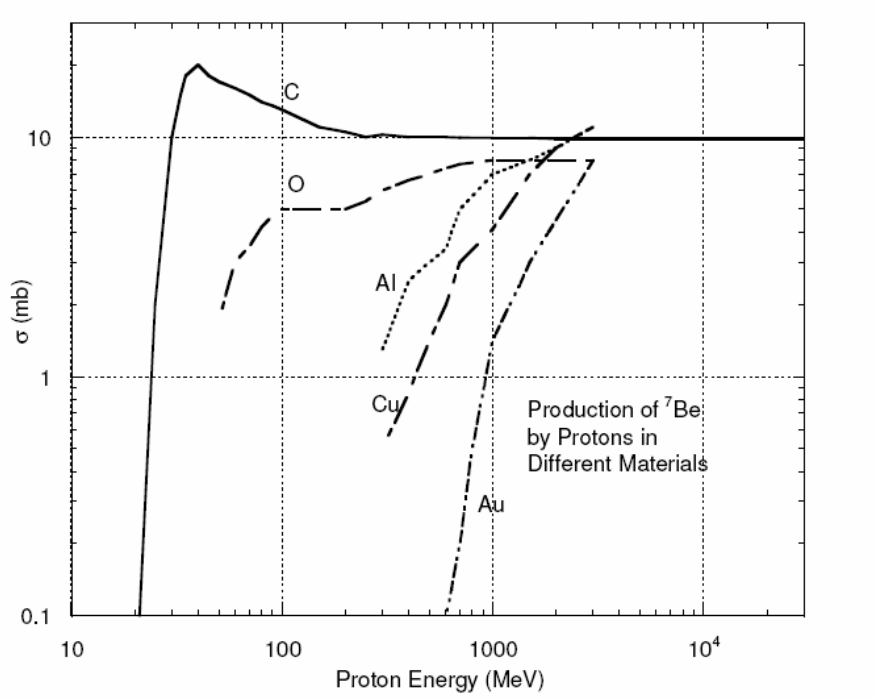
C
O
Al
Cu
Au
Production of ^{7}Be
by Protons in
Different Materials
σ (mb)
Proton Energy (MeV)
10
1
0.1
10
100
1000
10^4

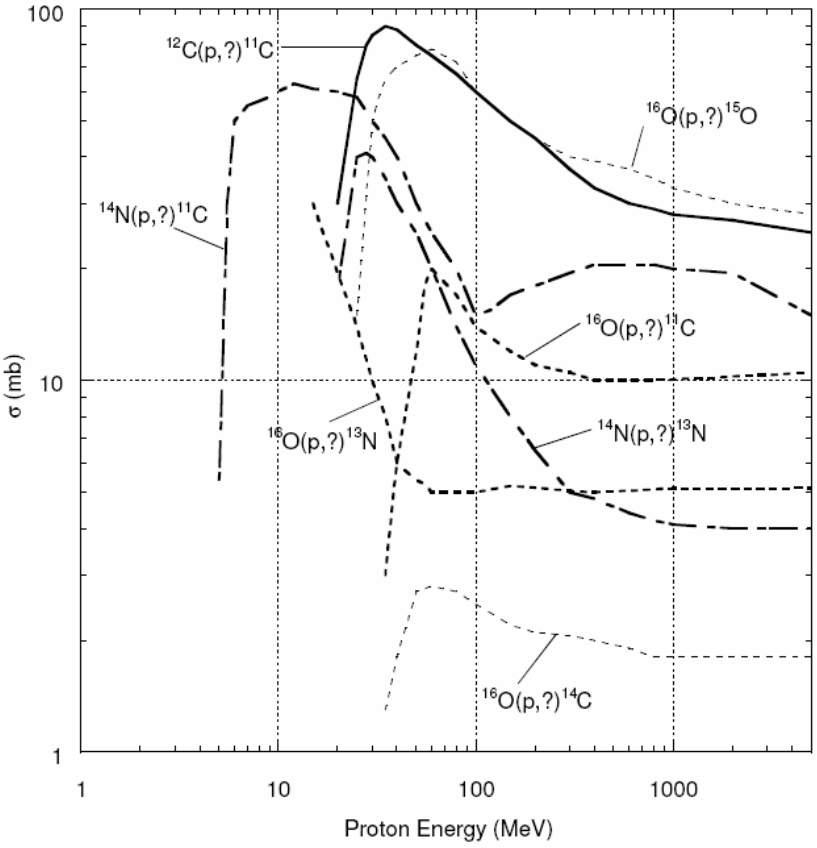
^{12}C(p,?)^{11}C
^{16}O(p,?)^{15}O
^{14}N(p,?)^{11}C
^{16}O(p,?)^{13}C
^{16}O(p,?)^{13}N
^{14}N(p,?)^{13}N
^{16}O(p,?)^{14}C
σ (mb)
Proton Energy (MeV)
100
10
1
1
10
100
1000

Fig. 5

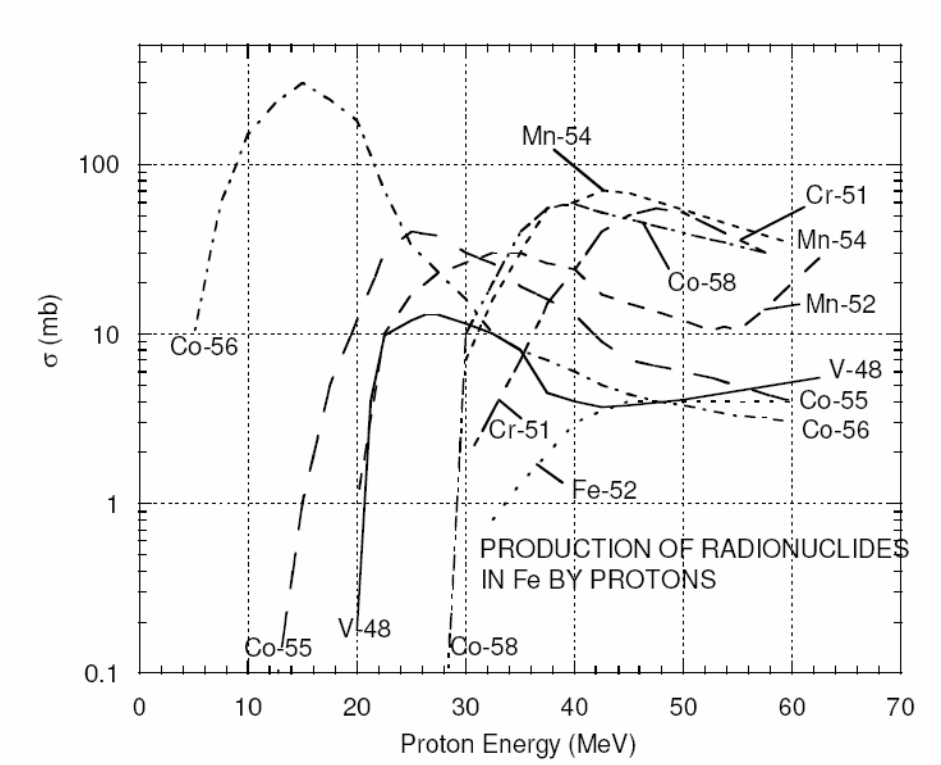
Mn-54
Cr-51
Mn-54
Co-58
Mn-52
Co-56
V-48
Co-55
Co-56
Cr-51
Fe-52
PRODUCTION OF RADIONUCLIDES
IN Fe BY PROTONS
V-48
Co-55
Co-58
σ (mb)
Proton Energy (MeV)

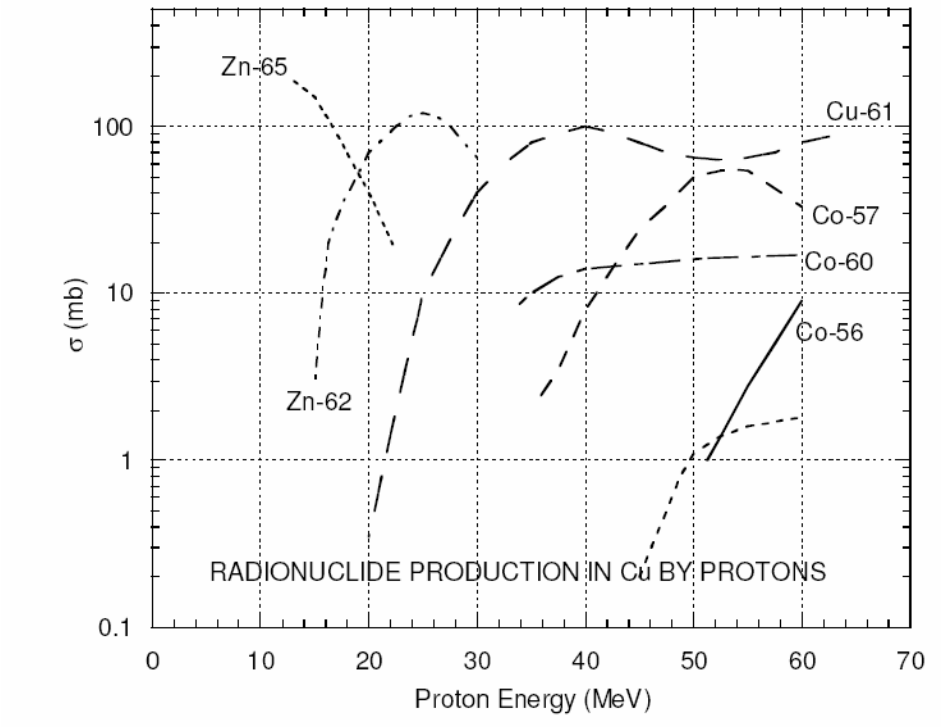
Zn-65
Cu-61
Co-57
Co-60
Co-56
Zn-62
RADIONUCLIDE PRODUCTION IN Cu BY PROTONS
σ (mb)
Proton Energy (MeV)

Fig. 6

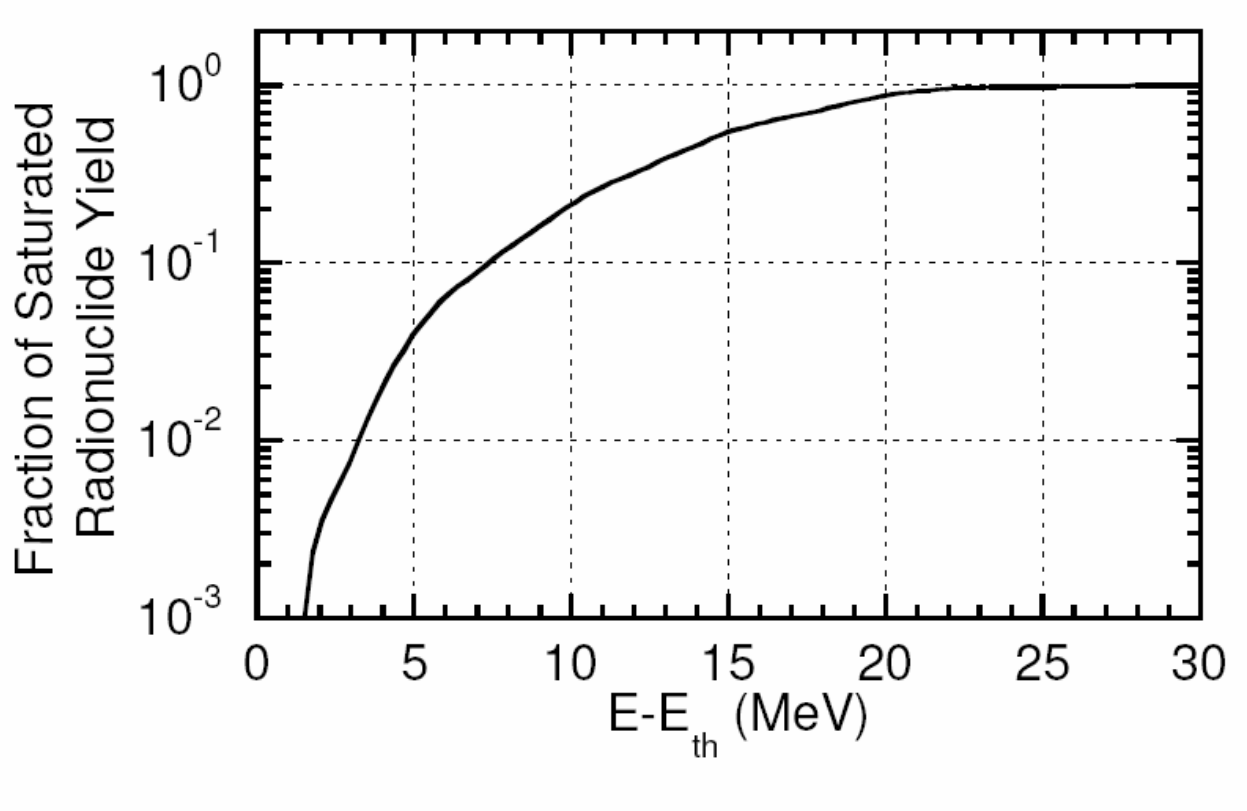
Fraction of Saturated Radionuclide Yield
10^0
10^-1
10^-2
10^-3
0
5
10
15
20
25
30
E-E_th (MeV)

Fig. 7

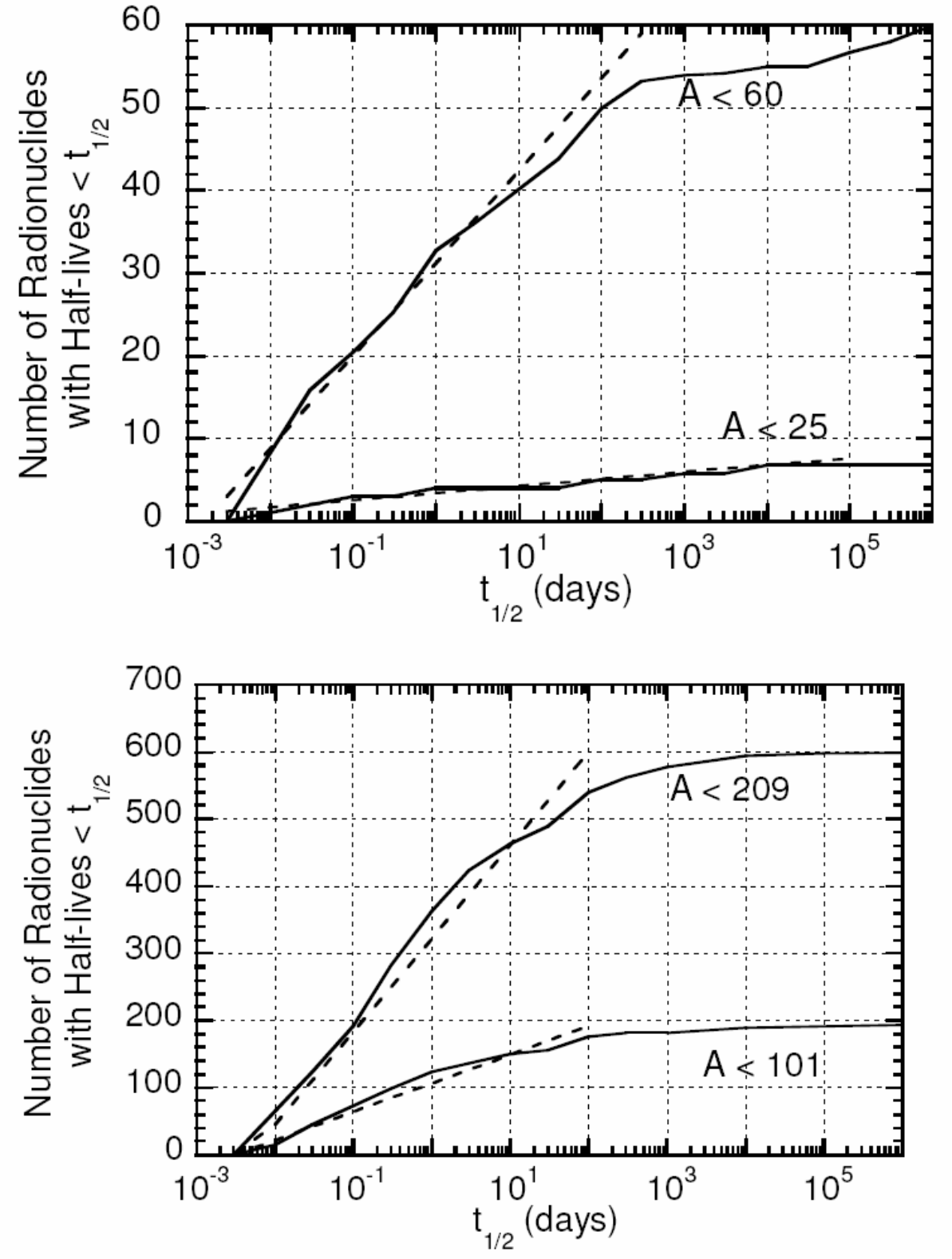
Number of Radionuclides with Half-lives < t1/2
A < 60
A < 25
t1/2 (days)
Number of Radionuclides with Half-lives < t1/2
A < 209
A < 101
t1/2 (days)

Fig. 8

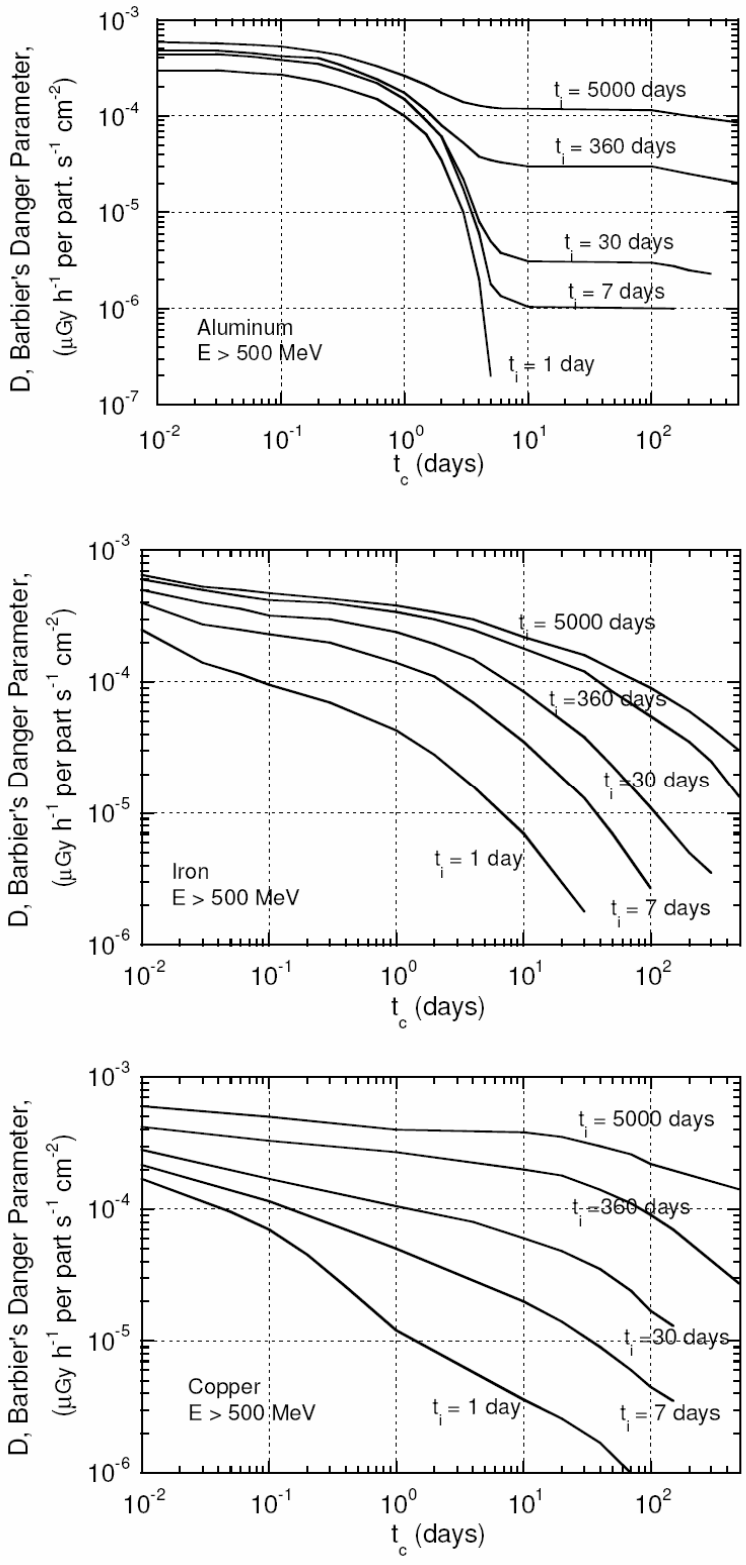
D, Barbier's Danger Parameter, (μGy h-1 per part. s-1 cm-2)
tc (days)
Aluminum
E > 500 MeV
ti = 5000 days
ti = 360 days
ti = 30 days
ti = 7 days
ti = 1 day
Iron
E > 500 MeV
ti = 5000 days
ti =360 days
ti =30 days
ti = 1 day
ti = 7 days
Copper
E > 500 MeV
ti = 5000 days
ti =360 days
ti =30 days
ti = 1 day
ti = 7 days

Fig. 9

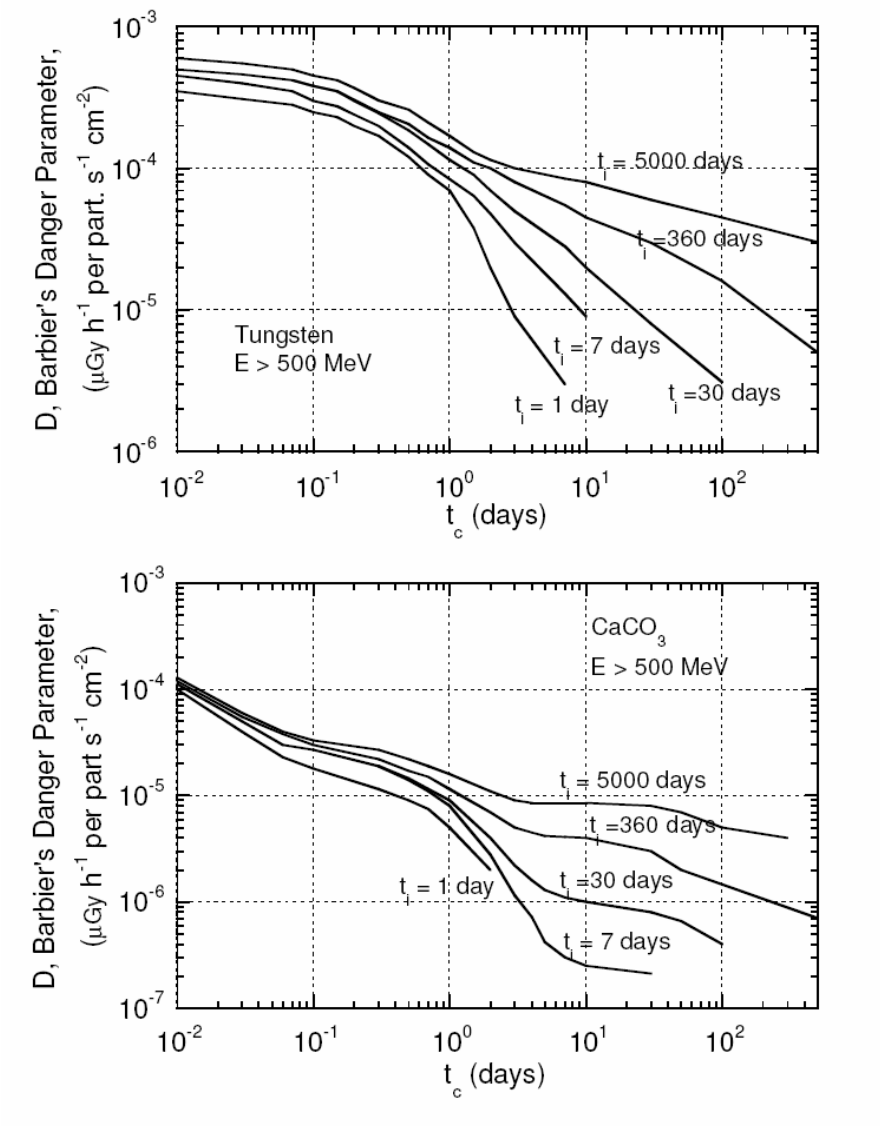
D, Barbier's Danger Parameter, (μGy h-1 per part. s-1 cm-2)
Tungsten
E > 500 MeV
ti = 5000 days
ti =360 days
ti = 7 days
ti = 1 day
ti =30 days
tc (days)
D, Barbier's Danger Parameter, (μGy h-1 per part s-1 cm-2)
CaCO3
E > 500 MeV
ti = 5000 days
ti =360 days
ti =30 days
ti = 1 day
ti = 7 days
tc (days)

Fig. 10

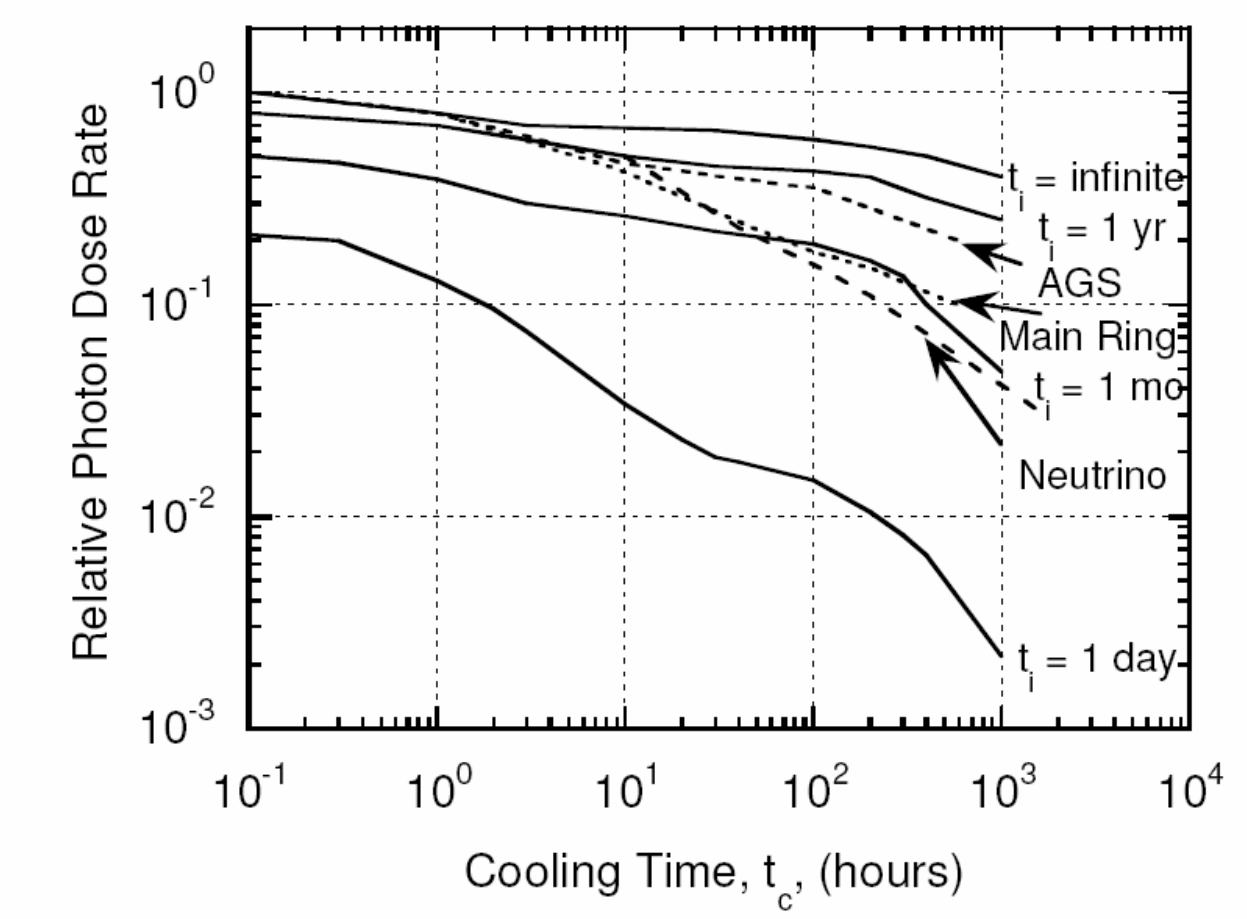
Relative Photon Dose Rate
10^{0}
10^{-1}
10^{-2}
10^{-3}
10^{-1}
10^{0}
10^{1}
10^{2}
10^{3}
10^{4}
Cooling Time, t_c, (hours)
t_i = infinite
t_i = 1 yr
AGS
Main Ring
t_i = 1 mo
Neutrino
t_i = 1 day

Fig. 11

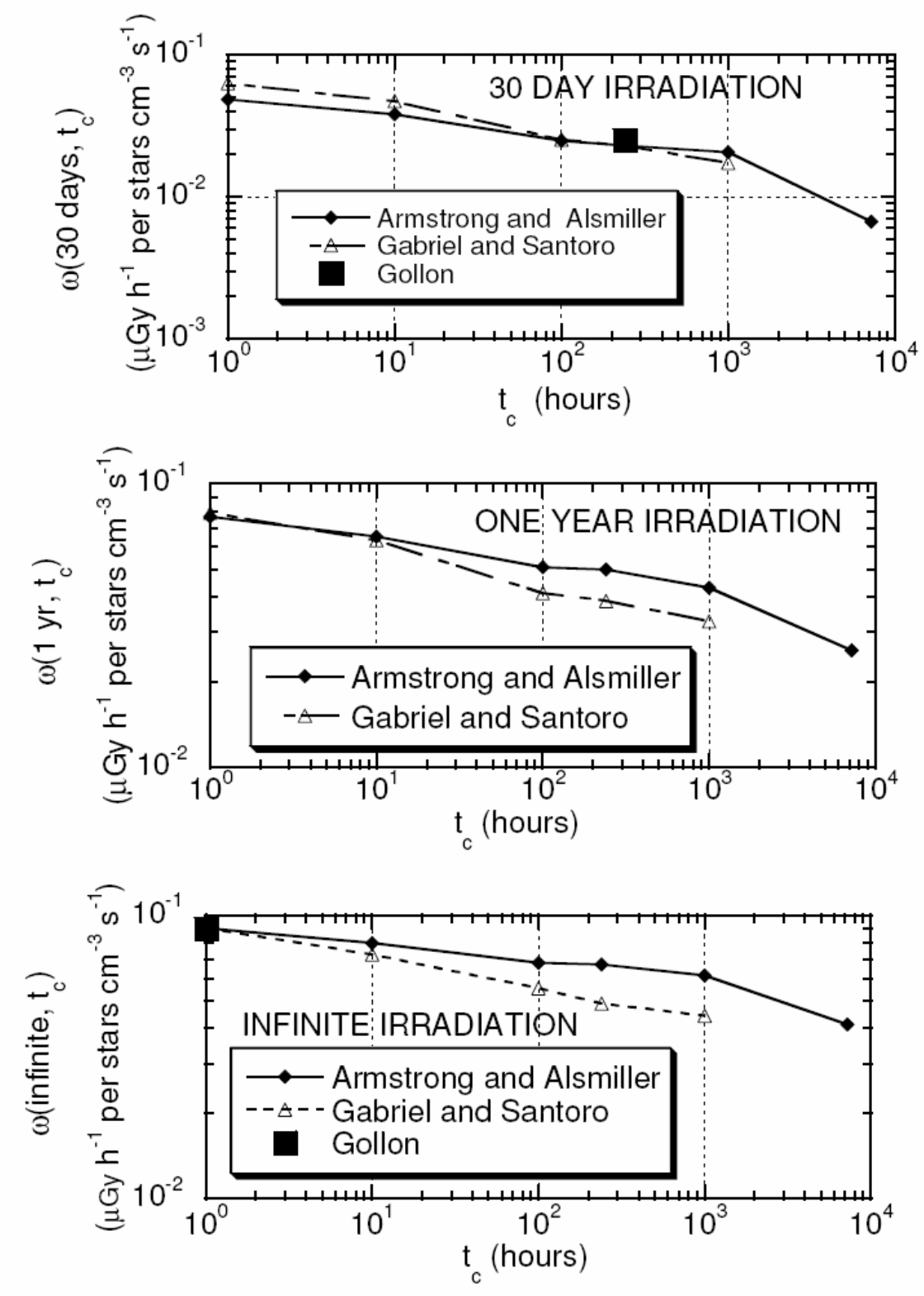
30 DAY IRRADIATION
ω(30 days, t_c)
(μGy h^-1 per stars cm^-3 s^-1)
Armstrong and Alsmiller
Gabriel and Santoro
Gollon
t_c (hours)
ONE YEAR IRRADIATION
ω(1 yr, t_c)
(μGy h^-1 per stars cm^-3 s^-1)
Armstrong and Alsmiller
Gabriel and Santoro
t_c (hours)
INFINITE IRRADIATION
ω(infinite, t_c)
(μGy h^-1 per stars cm^-3 s^-1)
Armstrong and Alsmiller
Gabriel and Santoro
Gollon
t_c (hours)

Fig. 12

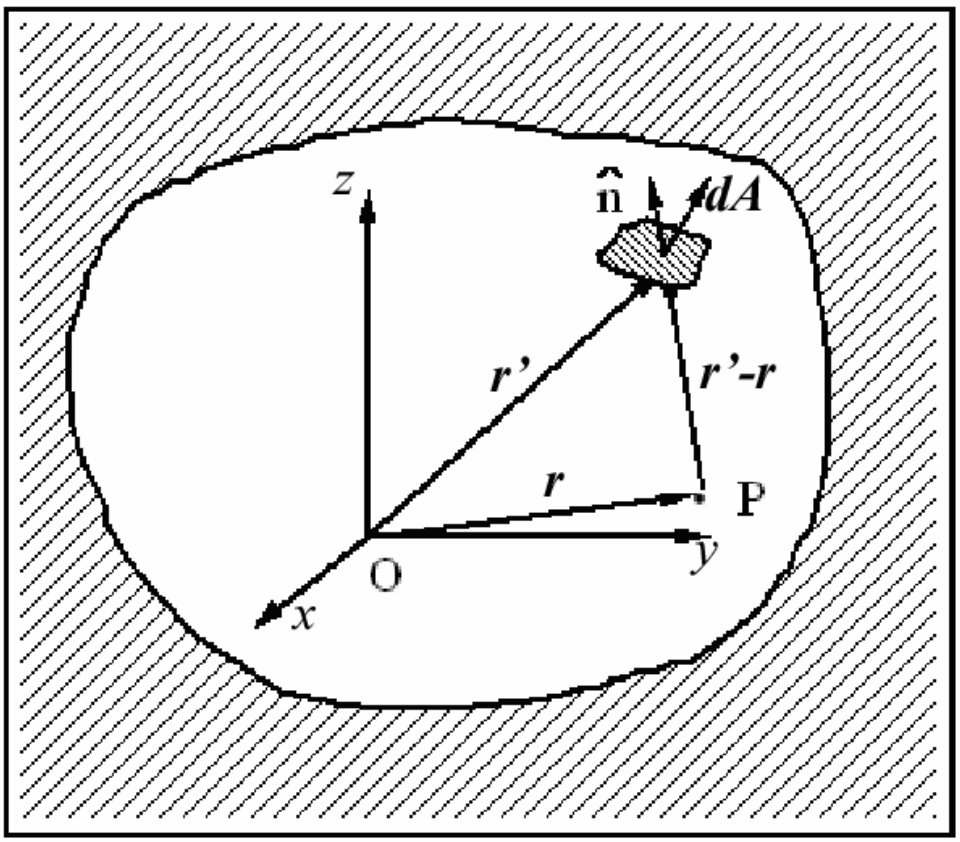

Fig. 13

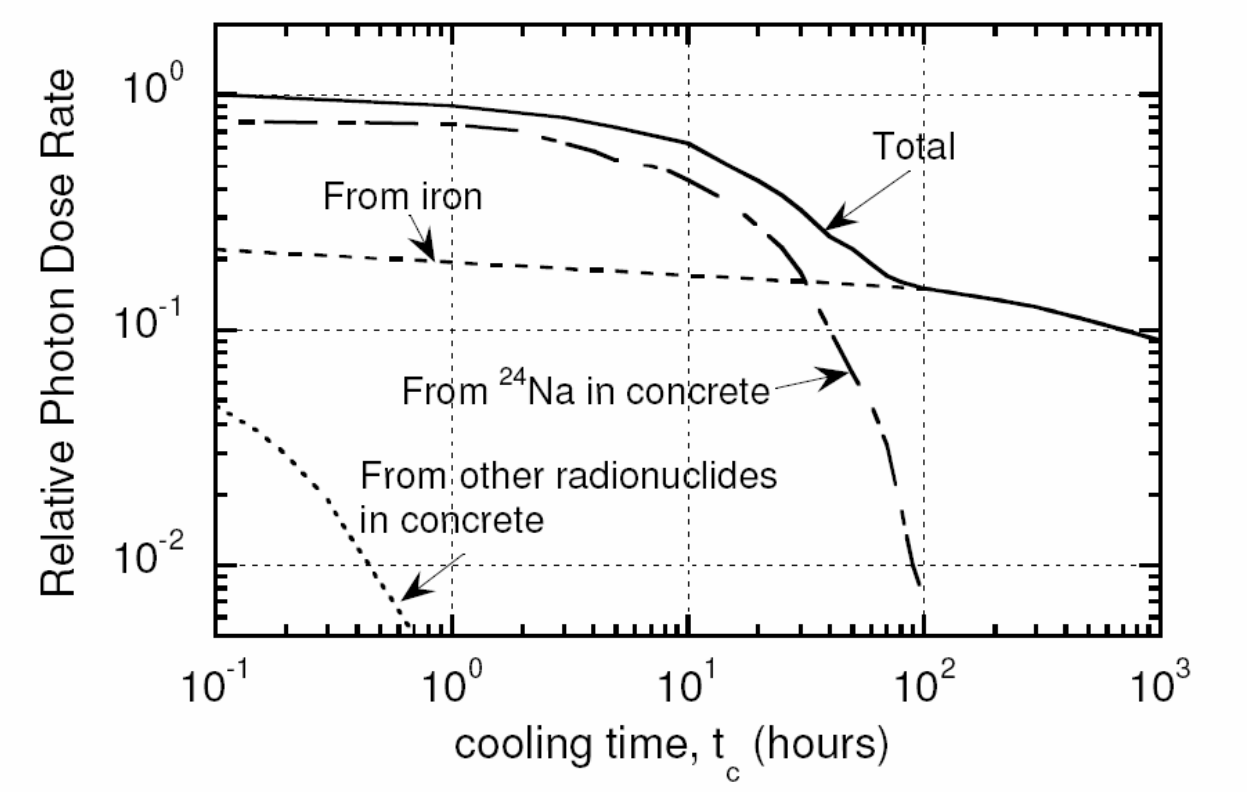
Relative Photon Dose Rate
10^0
10^{-1}
10^{-2}
Total
From iron
From ^{24}Na in concrete
From other radionuclides
in concrete
10^{-1}
10^0
10^1
10^2
10^3
cooling time, t_c (hours)

Fig. 14

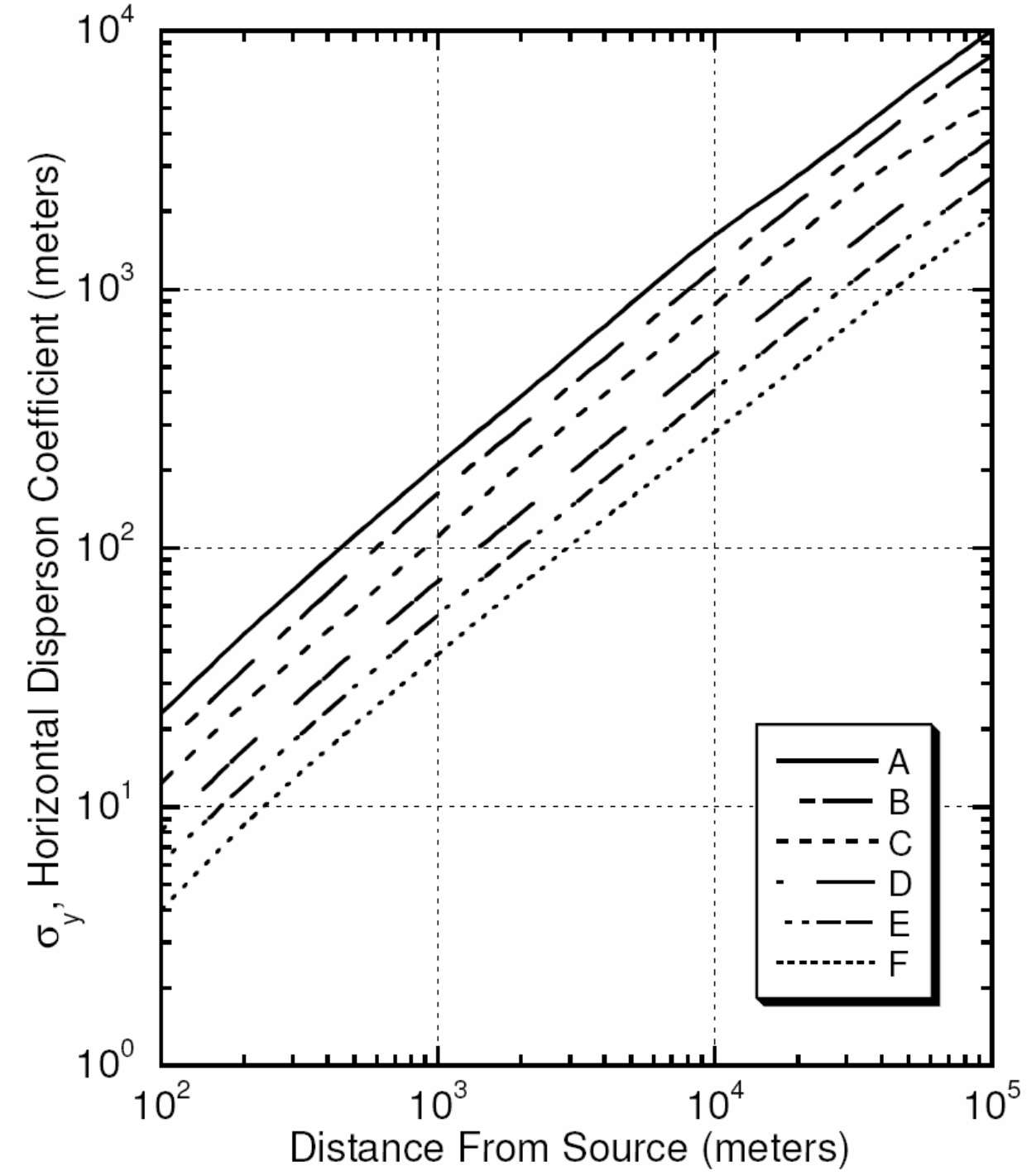
10^4
10^3
10^2
10^1
10^0
σ_y, Horizontal Disperson Coefficient (meters)
10^2
10^3
10^4
10^5
Distance From Source (meters)
A
B
C
D
E
F

Fig. 15

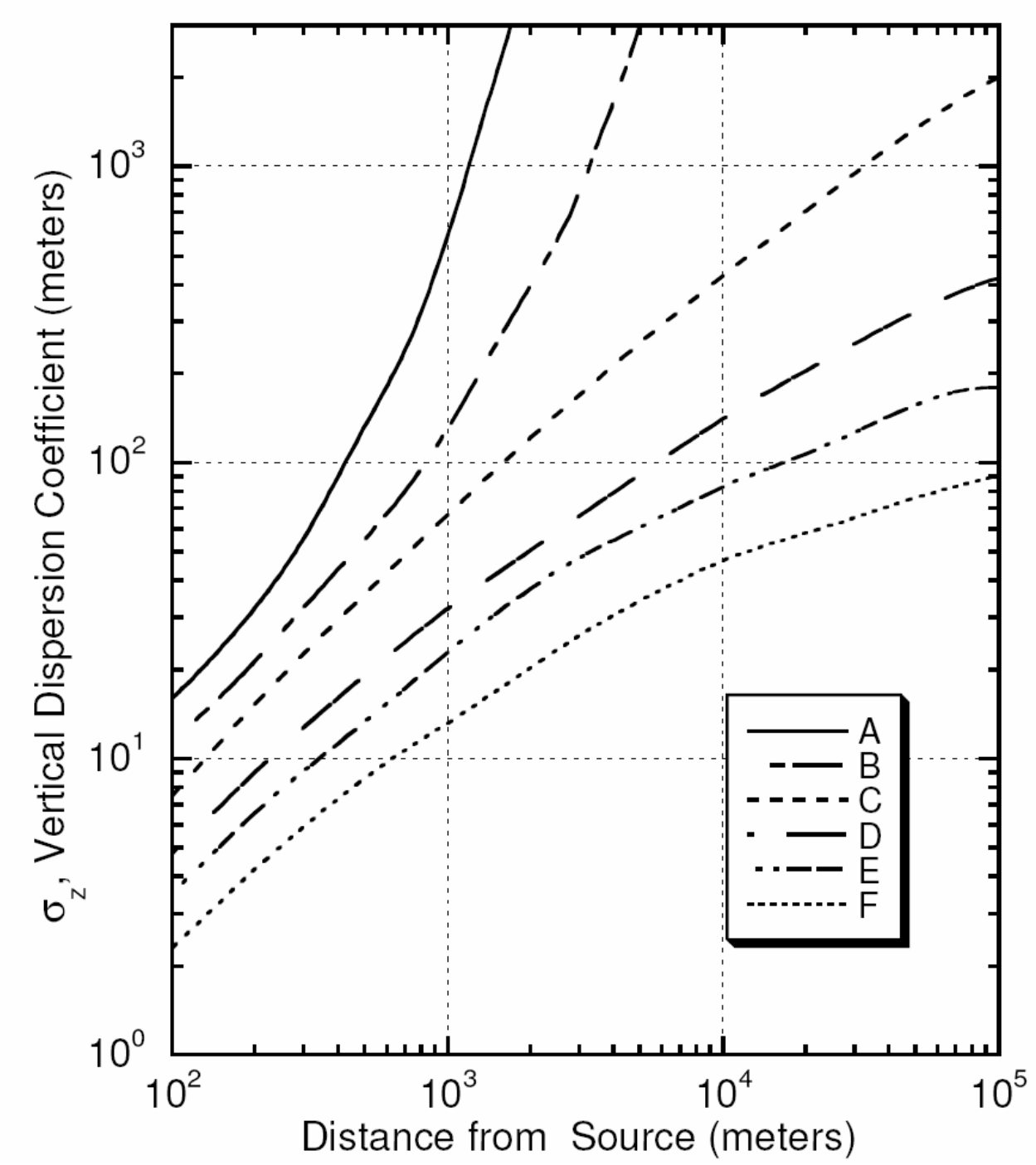
10^3
10^2
10^1
10^0
σ_z, Vertical Dispersion Coefficient (meters)
10^2
10^3
10^4
10^5
Distance from Source (meters)
A
B
C
D
E
F

Fig. 16

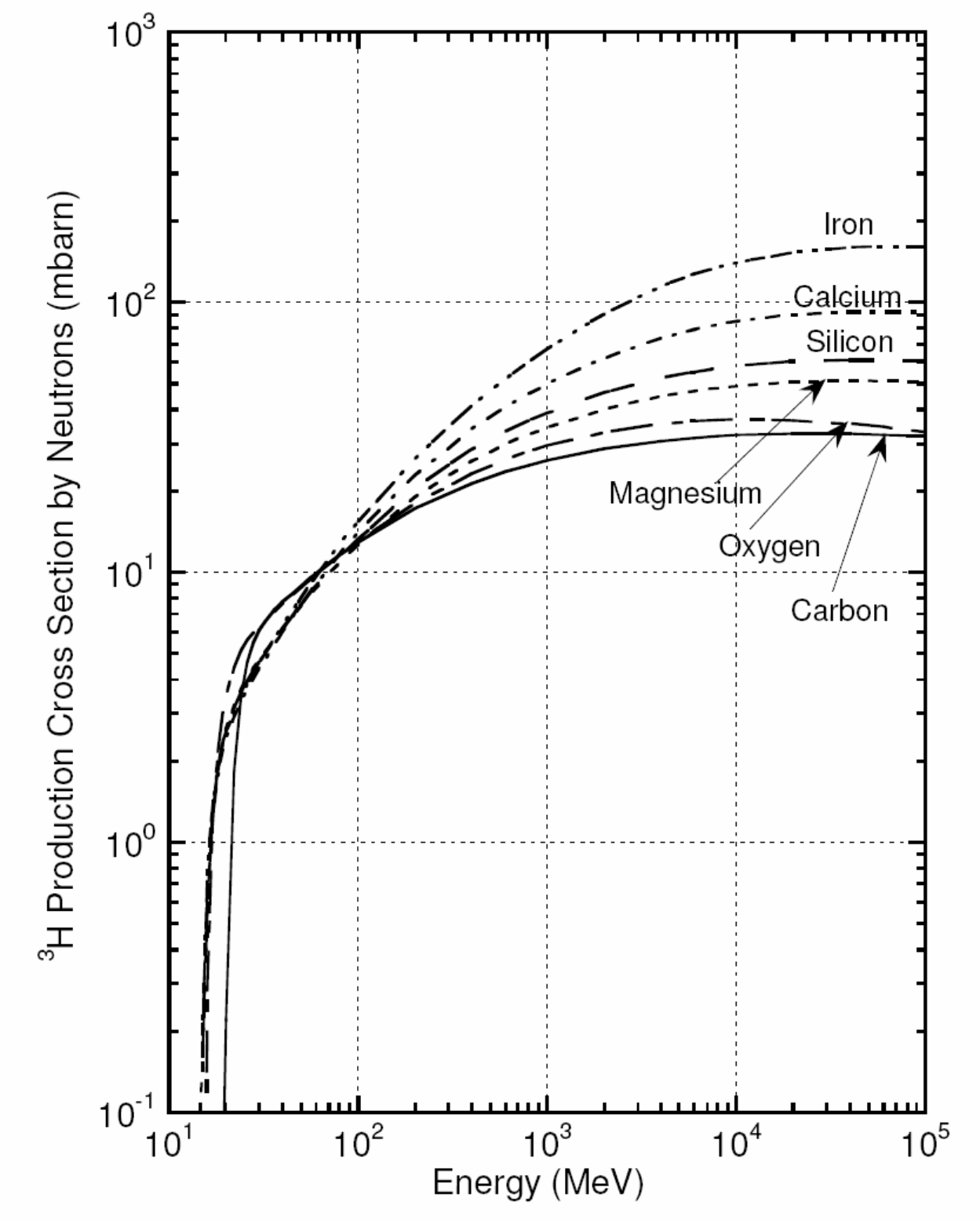
10^3
10^2
10^1
10^0
10^{-1}
^{3}H Production Cross Section by Neutrons (mbarn)
Iron
Calcium
Silicon
Magnesium
Oxygen
Carbon
10^1
10^2
10^3
10^4
10^5
Energy (MeV)

Fig. 17

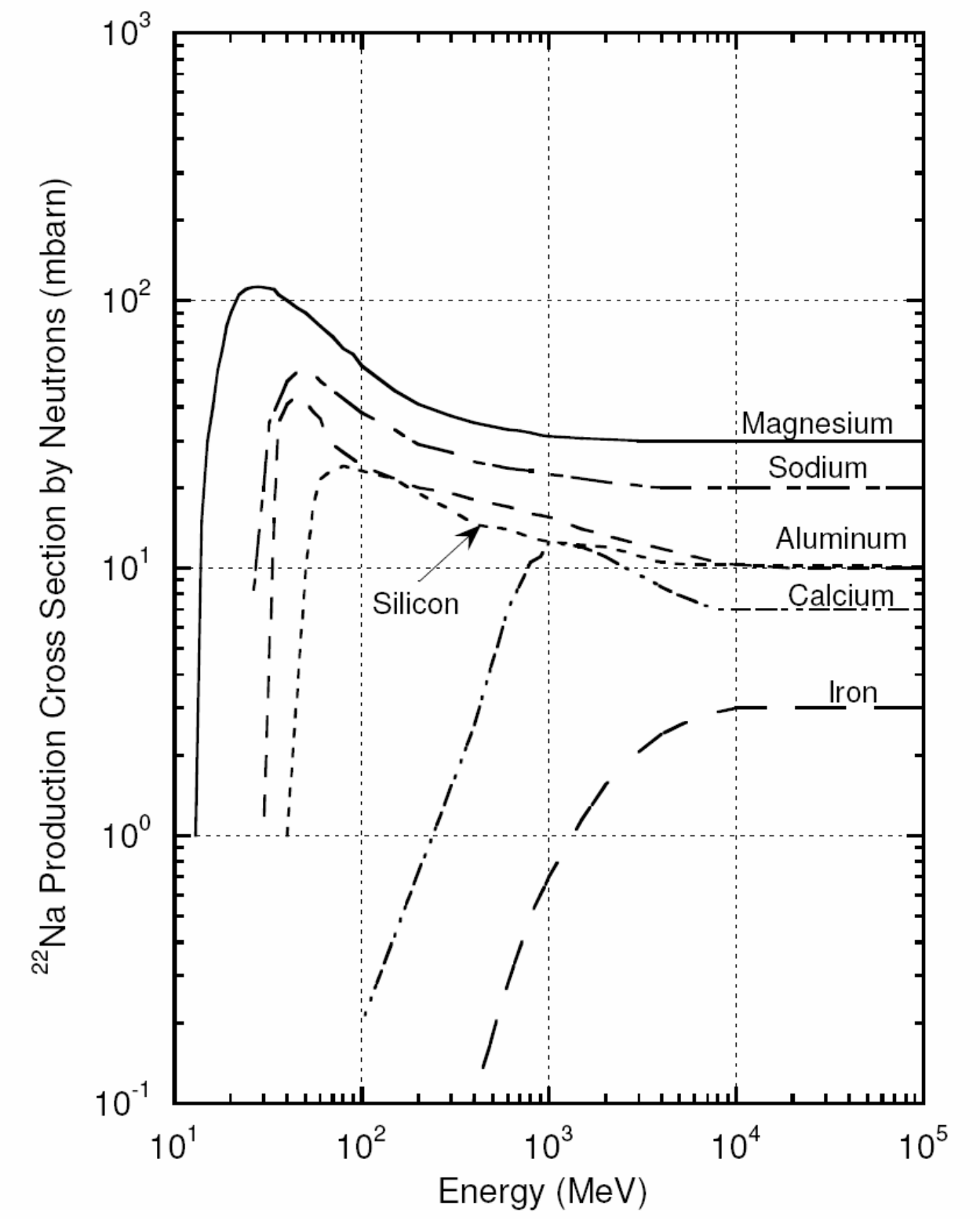
10^3
10^2
10^1
10^0
10^{-1}
^{22}Na Production Cross Section by Neutrons (mbarn)
Magnesium
Sodium
Aluminum
Silicon
Calcium
Iron
10^1
10^2
10^3
10^4
10^5
Energy (MeV)

Fig. 18

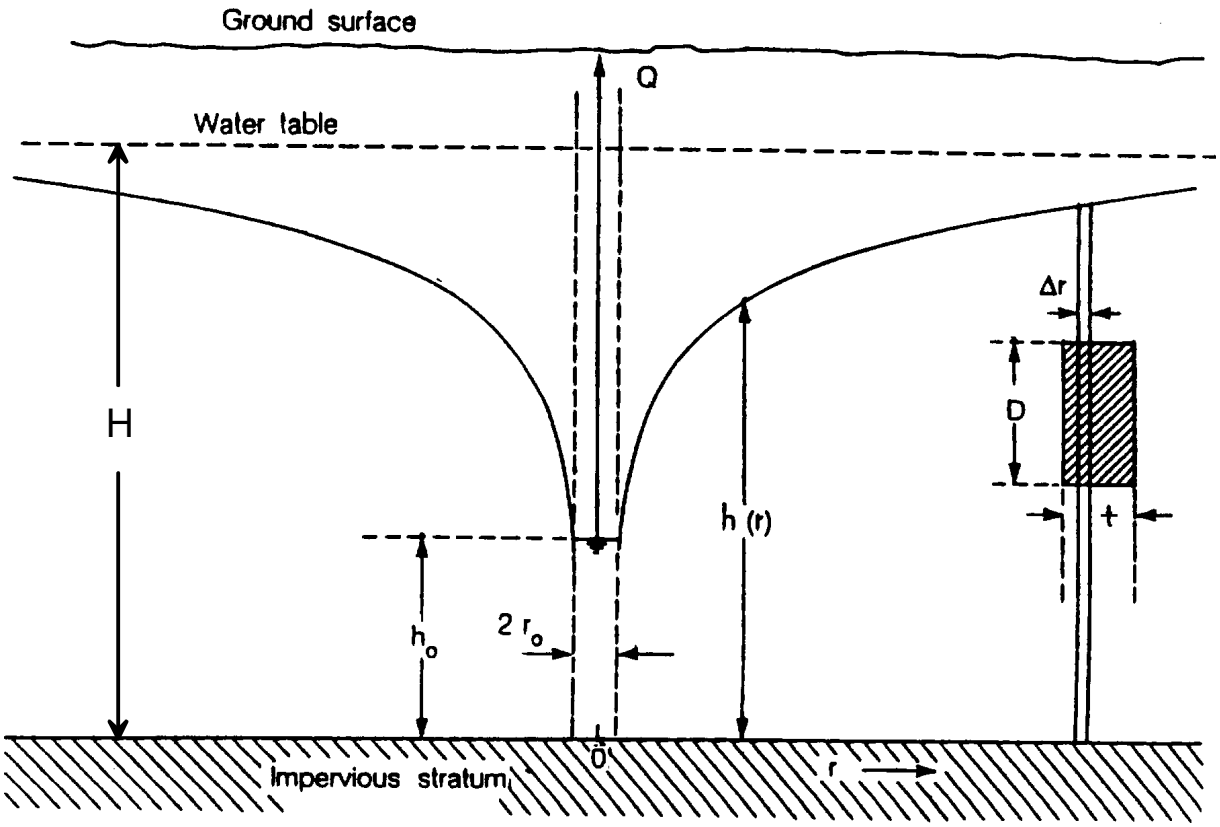
Ground surface
Q
Water table
H
Δr
D
h (r)
t
h_o
$2 r_o$
Impervious stratum
r

Fig. 19

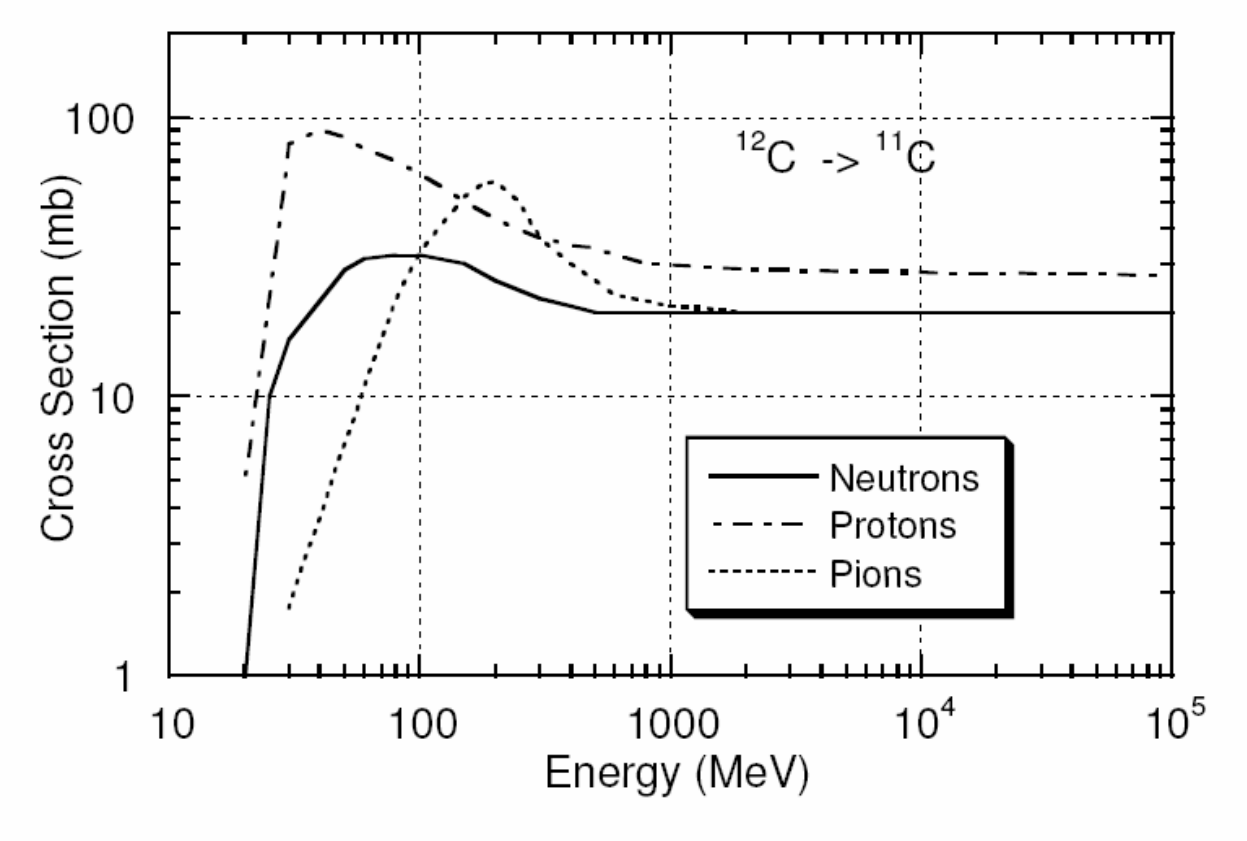
100
10
1
Cross Section (mb)
^{12}C -> ^{11}C
Neutrons
Protons
Pions
10
100
1000
10^4
10^5
Energy (MeV)

Fig. 20

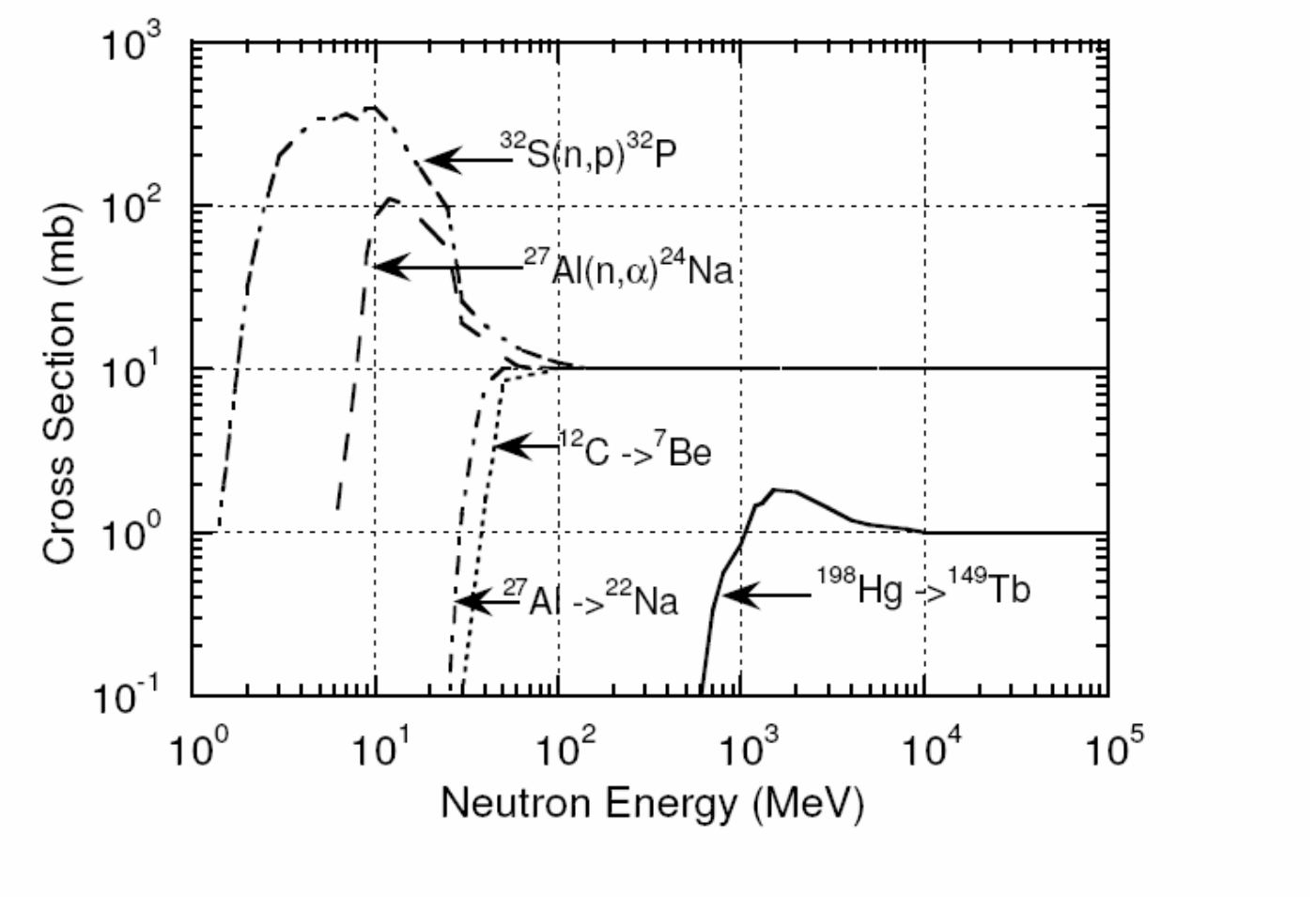
Cross Section (mb)
Neutron Energy (MeV)
$^{32}S(n,p)^{32}P$
$^{27}Al(n,\alpha)^{24}Na$
$^{12}C \rightarrow ^{7}Be$
$^{27}Al \rightarrow ^{22}Na$
$^{198}Hg \rightarrow ^{149}Tb$

Fig. 21

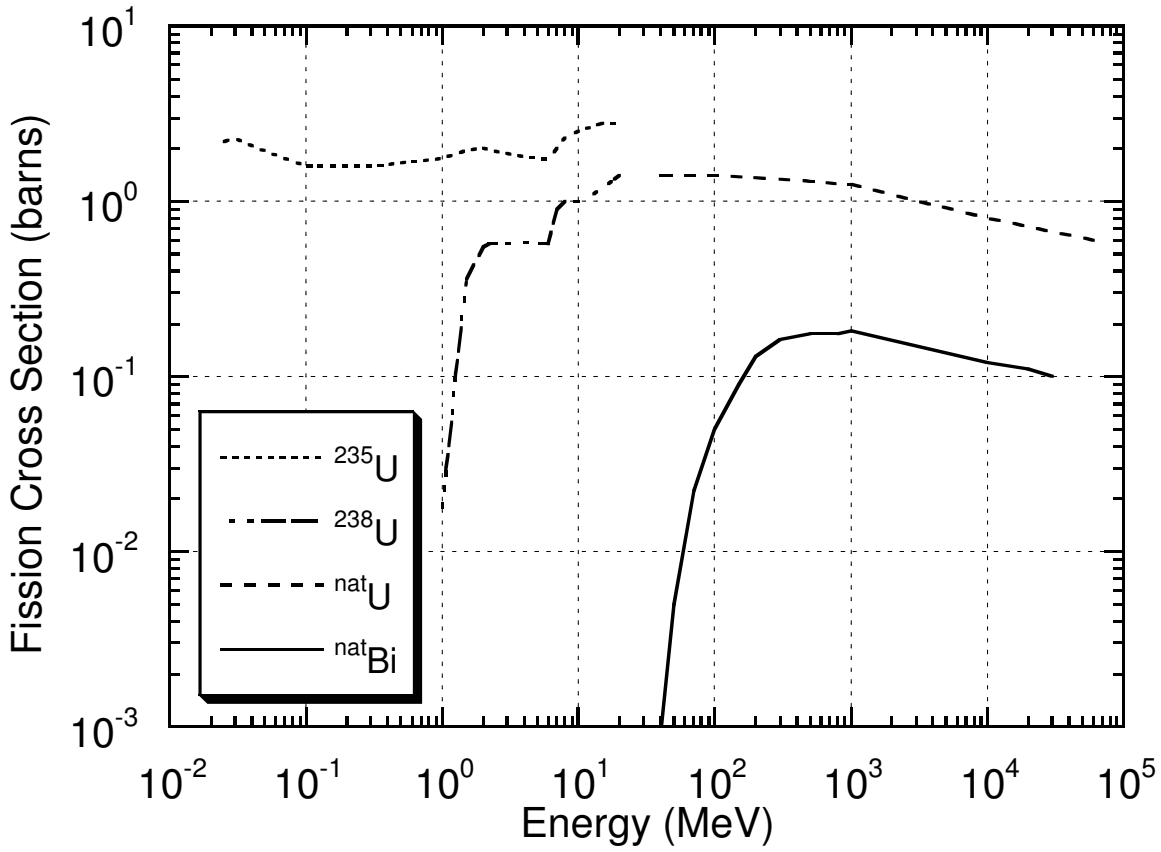
Fission Cross Section (barns)
Energy (MeV)
10^{1}
10^{0}
10^{-1}
10^{-2}
10^{-3}
10^{-2}
10^{-1}
10^{0}
10^{1}
10^{2}
10^{3}
10^{4}
10^{5}
^{235}U
^{238}U
^{nat}U
^{nat}Bi